Mixed finite elements for solving 2-d diffusion-type equations

A. Younes, P. Ackerer, F. Delay

MIXED FINITE ELEMENTS FOR SOLVING 2-D DIFFUSION-TYPE EQUATIONS

Anis Younes,[1] Philippe Ackerer,[1] and Frederick Delay[2]

Received 1 October 2008; revised 16 July 2009; accepted 28 September 2009; published 31 March 2010.

[1] Mixed finite elements are a numerical method becoming more and more popular in geosciences. This method is well suited for solving elliptic and parabolic partial differential equations, which are the mathematical representation of many problems, for instance, flow in porous media, diffusion/dispersion of solutes, and heat transfer, among others. Mixed finite elements combine the advantages of finite elements by handling complex geometry domains with unstructured meshes and full tensor coefficients and advantages of finite volumes by ensuring mass conservation at the element level. In this work, a physically based presentation of mixed finite elements is given, and the main approximations or reformulations made to improve the efficiency of the method are detailed. These approximations or reformulations exhibit links with other numerical methods (nonconforming finite elements, finite differences, finite volumes, and multipoint flux methods). Some improvements of the mixed finite element method are suggested, especially to avoid oscillations for transient simulations and distorted quadrangular grids.

Citation: Younes, A., P. Ackerer, and F. Delay (2010), Mixed finite elements for solving 2-D diffusion-type equations, *Rev. Geophys.*, *48*, RG1004, doi:10.1029/2008RG000277.

1. INTRODUCTION

[2] We consider the numerical solution of the following 2-D diffusion-type partial differential equations (PDEs):

$$c\frac{\partial h}{\partial t} + \nabla \cdot \mathbf{q} = f \quad \text{in } \Omega, \tag{1}$$

$$\mathbf{q} = -\mathbf{K}\nabla h, \tag{2}$$

$$h = h_D \quad \text{on } \partial\Omega_D,$$

$$\mathbf{K}\frac{\partial h}{\partial \mathbf{n}} = g \quad \text{on } \partial\Omega_N,$$

where Ω is a bounded polygonal open set of $\mathbb{R}^2$, $\partial\Omega_D$ and $\partial\Omega_N$ are partitions of the boundary $\partial\Omega$ of Ω corresponding to Dirichlet and Neumann conditions, and $\mathbf{n}$ is the unit outward vector normal to the boundary $\partial\Omega$.

[3] The system of PDEs (1) and (2) and its associated boundary conditions are a very common mathematical model in geosciences. Equation (1) states the conservation principle, and (2) is a constitutive law like Fourier's law, Fick's law, Ohm's law, or Darcy's law. In the context of flow in porous media considered in this paper, the state variable h corresponds to the pressure head (L), $\mathbf{K}$ is the symmetric positive definite conductivity tensor ($L\ T^{-1}$), c is the storage coefficient (L^{-1}), and f is the sink/source term (T^{-1}). The components of $\mathbf{K}$ are assumed to be bounded, but $\mathbf{K}$ may be highly anisotropic and/or discontinuous. Indeed, full parameter tensors often appear for flow in natural porous media when the orientation of the calculation grid does not match up eventual anisotropic features of the geological settings.

[4] A standard way to solve the system (1) and (2) is to substitute Darcy's equation (2) in the mass conservation equation (1) and then solve the resulting form with the standard finite element method. However, this approach yields fluid fluxes with discontinuous normal components across interfaces between adjacent elements. In the presence of a heterogeneous permeability field, these discrepancies result in inaccurate fluid velocities [*Durlofsky*, 1994], which, in turn, lead to inaccurate characterization of the fate of chemical species [*Dawson*, 1999]. Note, however, that postprocessing techniques can be employed to enhance the velocity field approximation [*Cordes and Kinzelbach*, 1992; *Loula et al.*, 1995; *Hughes et al.*, 2000; *Correa and Loula*, 2007].

[5] The system (1) and (2) can also be solved with standard finite volume methods. However, standard finite

[1]Laboratoire d'Hydrologie et de Géochimie de Strasbourg, EOST, Université de Strasbourg, CNRS, Strasbourg, France.
[2]UMR 6532, University of Poitiers, CNRS, Poitiers, France.

volumes can generate significant errors when applied to unstructured grids and/or in the presence of full-tensor coefficients [*Chen et al.*, 2008; *Wu and Parashkevov*, 2005].

[6] The mixed finite element (MFE) method [*Raviart and Thomas*, 1977; *Brezzi et al.*, 1985; *Chavent and Jaffré*, 1986; *Brezzi and Fortin*, 1991] is an alternative method which combines the advantages of finite volumes and finite elements: (1) The method is locally conservative at the element level: the sum of the fluxes over all edges of each cell discretizing the domain equals the accumulation term plus any sources or sinks in the cell. (2) The fluxes are continuous between adjacent cells. (3) Unstructured grids can be handled. (4) Anisotropic discontinuous conductivity tensors are treated in a consistent way, like with finite elements. Note that recently, other conservative numerical methods for flow in porous media have been developed [*Edwards*, 2002], such as the control volume mixed finite element method [*Cai et al.*, 1997; *Klausen and Russell*, 2005], the support operator method [*Hyman et al.*, 1997; *Berndt et al.*, 2001], the multipoint flux approximation method [*Aavatsmark et al.*, 1994; *Edwards and Rogers*, 1994, 1998; *Aavatsmark*, 2002], and the mimetic finite difference method [*Kuznetsov et al.*, 2004; *Brezzi et al.*, 2005a, 2005b; *Lipnikov et al.*, 2006].

[7] The original idea for MFEs emanated from structural mechanics [*Herrman*, 1967]. Since then, it has been developed for a wide variety of fields including Stokes's problems [*Girault and Raviart*, 1986], flow in porous media [*Chavent and Jaffré*, 1986], and electromagnetism [*Nédélec*, 1980; *Bossavit*, 1988]. The method has been extensively employed during the last 20 years [e.g., *Darlow et al.*, 1984; *Brezzi and Fortin*, 1991; *Bergamaschi et al.*, 1994; *Mosé et al.*, 1994; *Ackerer et al.*, 1999; *Younes et al.*, 1999a; *Chavent et al.*, 2003; *Arbogast and Boyd*, 2006].

[8] In the field of water resources, applicability and worth of MFEs were shown for a wide range of problems, including steady state [*Arbogast et al.*, 1997; *Chavent and Roberts*, 1991; *Durlofsky*, 1994; *James and Graham*, 1999] and transient [*Chavent and Roberts*, 1991; *Ackerer et al.*, 1999; *Younes et al.*, 1999a] single-phase flow, flow in unsaturated media [*Farthing et al.*, 2003], multiphase flow [*Chen and Ewing*, 1997; *Dawson et al.*, 1998; *Bergamaschi and Putti*, 1999; *Huber and Helmig*, 1999; *Nayagum et al.*, 2004; *Hoteit and Firoozabadi*, 2008], flow with heat transfer [*Chounet et al.*, 1999; *Holstad*, 2001], multiphase flow in fractured media [*Hoteit and Firoozabadi*, 2005, 2008], and numerical upscaling [*Durlofsky*, 1998; *Ma et al.*, 2006]. The MFE method was also successfully used to obtain a locally mass conservative multiscale approach. The developments are deeply documented by, e.g., *Arbogast* [2000, 2002, 2004], *Arbogast and Boyd* [2006], *Chen and Hou* [2002], *Aarnes* [2004], *Aarnes et al.* [2005], *Kippe et al.* [2008], and *Juanes and Dub* [2008].

[9] Basically, MFEs simultaneously solve both pressure head and velocity fields by representing each unknown with its own space of basis functions. Therefore, the velocity field is directly approximated by the basis functions of finite elements, which can be much more accurate than solving for the heads first and then getting velocity by local numerical evaluations of $\mathbf{K} \cdot \nabla h$ [*Ewing and Heinemann*, 1983].

[10] From a mathematical standpoint, the MFE method is reputed to be superconvergent for both velocity and pressure head when smooth permeability fields and smooth grids are used [*Wang and Mathew*, 1994; *Ewing et al.*, 1999]. In heterogeneous media, the MFE velocities are substantially more accurate than those obtained with standard methods [*Chavent et al.*, 1984; *Durlofsky*, 1994; *Mosé et al.*, 1994; *Ackerer et al.*, 1996]. The merits of MFEs were proved by comparisons with conforming finite element [*Mosé et al.*, 1994; *Huber and Helmig*, 1999] and control volume finite element discretizations [*Durlofsky*, 1994]. Specifically, *Durlofsky* [1994] showed the accuracy of fluid velocities and related quantities (stream function and flux) from MFEs compared with control volume finite element methods. He showed that MFEs provided more accurate solutions for total flux and stream function, for the same amount of computational effort, than the control volume finite element method. *Matringe et al.* [2006] also pointed out reliability and worth of MFEs for streamline tracing as the consequence of the rigorous approximation of the velocity field.

[11] The MFE method requires more unknowns than standard finite elements or finite volumes. As reported in the ongoing literature, many authors have tried to reduce the number of unknowns of MFEs to decrease computation times. These manipulations revealed links and similarities between MFE and finite volume methods [e.g., *Russell and Wheeler*, 1983; *Baranger et al.*, 1994; *Arbogast et al.*, 1997; *Younes et al.*, 1999b; *Cai et al.*, 2003].

[12] In this work, we focus on 2-D problems with unstructured triangular and quadrangular grids. In section 2, we give a physically based presentation of the MFE method and its hybridization. Developments are provided for lowest-order mixed methods of *Raviart and Thomas* [1977] (Raviart-Thomas elements of zero order (RT0)) and *Brezzi et al.* [1985] (Brezzi-Douglas-Marini elements of first order (BDM1)) since these methods are frequently used for practical applications. Alternative formulations developed to reduce the number of unknowns are described in section 3, and relationships with other methods like finite volumes or multipoint flux approximations are shown in section 4. Section 5 discusses the behavior of MFE solutions for steady state problems with heterogeneous and anisotropic diffusion tensors. Some improvements for transient simulations and for distorted quadrangular grids are also proposed to improve stability of the MFE method. Finally, streamline tracing with both RT0 and BDM1 is discussed in section 6.

2. GENERAL FORMULATION OF THE MIXED AND MIXED HYBRID FINITE ELEMENT METHOD

[13] MFEs and the hybridized form (mixed hybrid finite element (MHFE) methods) are presented separately. This deliberate choice is made for the sole purpose of clearly describing two main ways of writing the discrete equations of the same problem. Though these writings have some

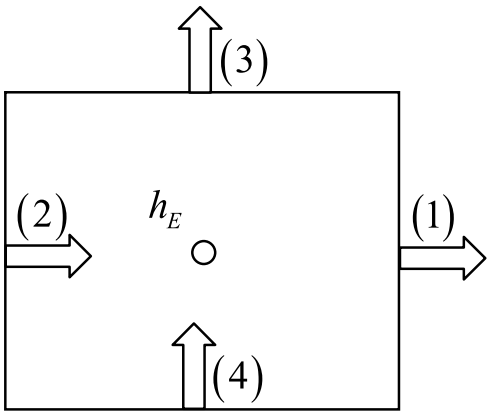

Figure 1. Flux orientations and edge numbering for a rectangular element.

incidence on numerical resolutions, from a formal standpoint MFEs and MHFEs are equivalent.

2.1. Standard Mixed Finite Element Method

[14] In this section, formalisms for both RT0 and BDM1 are developed over unstructured 2-D triangular and quadrangular meshes. The standard formulations of RT0 and BDM1 lead to poorly conditioned symmetric indefinite linear systems, particularly for steady state conditions [*Golub and Van Loan*, 1989; *Brezzi and Fortin*, 1991]. This prevents the use of efficient iterative solvers based on conjugate gradient methods. To make this point clear and also to illustrate how the standard MFE method works, the developments in sections 2.1.1–2.1.3 are limited to the standard RT0 formulation for the elliptic case ($c = 0$ in (1)) over a rectangular meshing. Note, however, that the method can also be applied to the transient case ($c \neq 0$ in (1)) and over elements of various shapes. With regard to its philosophy, the presentation of the MFE method detailed in sections 2.1.1–2.1.3 is similar to the physically based developments proposed by *Chavent and Roberts* [1991].

2.1.1. Approximation Spaces

[15] With MFEs, mass conservation (1) and Darcy's law (2) are approximated individually. With RT0, the pressure head is considered to be piecewise constant over each element. The velocity components are attached to the edges of the elements and are considered to be piecewise linear:

$$h = \sum_{E=1}^{\mathrm{Ne}} h_E \Gamma_E, \tag{3}$$

$$\mathbf{q} = \sum_{i=1}^{\mathrm{Ned}} Q_i \boldsymbol{\omega}_i(x,y), \tag{4}$$

where Ne is the total number of elements, Ned is the total number of element edges, and $\Gamma_E = 1$ over element E and 0 elsewhere. Q_i are the degrees of freedom of the velocity, which correspond to the fluxes across the edges (the zero-order moment of the normal flux). Because the degrees of freedom are shared between two adjacent elements, they must be defined with the same orientation. It is therefore convenient to orientate $\mathbf{n}_j$, the vector normal to the edge j, along x positive for vertical edges and along y positive for horizontal edges (Figure 1).

[16] The velocity in (4) is approximated by using vector basis functions $\boldsymbol{\omega}_i$ (x, y), i.e., vectors of the RT0 space [*Raviart and Thomas*, 1977; *Thomas*, 1977] which verify on the edge j:

$$\int_j \boldsymbol{\omega}_i \cdot \mathbf{n}_j = \delta_{ij} \qquad j = 1, \ldots, \mathrm{Ned}, \tag{5}$$

where δ_{ij} is the Kronecker symbol ($\delta_{ij} = 1$ for $j = i$ and $\delta_{ij} = 0$ otherwise). Equation (5) implies that the basis function $\boldsymbol{\omega}_i$ has a continuous normal component at the edge i and is nonzero only over the two elements E and E' sharing i.

[17] For example, a vertical edge i shared by two elements E and E' has its corresponding vector basis function $\boldsymbol{\omega}_i$ given by (see Figure 2)

$$\boldsymbol{\omega}_i = \begin{cases} \boldsymbol{\omega}_{E,i} = \dfrac{1}{|E|}\begin{pmatrix} x - x_{i-1} \\ 0 \end{pmatrix} & \text{on } E \\ \boldsymbol{\omega}_{E',i} = \dfrac{1}{|E'|}\begin{pmatrix} x_{i+1} - x \\ 0 \end{pmatrix} & \text{on } E' \\ 0 \qquad \text{elsewhere,} \end{cases} \tag{6}$$

where $|E|$ and $|E'|$ are the areas of elements E and E', respectively.

2.1.2. Discretization of Darcy's Law and the Mass Balance Equation

[18] Darcy's law (2) can be rewritten in the form $\mathbf{K}^{-1}\mathbf{q} + \nabla h = 0$ and expressed in a variational form like with finite elements. This leads to

$$\int_\Omega \mathbf{K}^{-1}\mathbf{q}\boldsymbol{\omega}_i + \int_\Omega \nabla h\, \boldsymbol{\omega}_i = 0. \tag{7}$$

Integrating by parts the second term of (7) and using (3) and (4) gives

$$\sum_{j=1}^{\mathrm{Ned}} Q_j \int_\Omega \left(\mathbf{K}^{-1}\,\boldsymbol{\omega}_j\right)\boldsymbol{\omega}_i - \sum_{E=1}^{\mathrm{Ne}} h_E \int_\Omega \nabla\boldsymbol{\omega}_i\,\Gamma^E + h_D \int_{\partial\Omega_D} \boldsymbol{\omega}_i\,\mathbf{n}_{\partial\Omega_D} = 0. \tag{8}$$

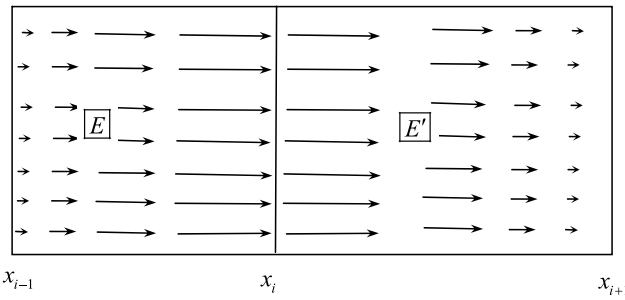

Figure 2. The vector basis function $\boldsymbol{\omega}_i$ for a vertical edge separating two adjacent elements E and E'.

[19] This equation is written for all the edges inside the domain (thus separating adjacent elements) and for boundary edges with a prescribed Dirichlet condition (where the head is fixed to h_D). For an interior edge, $\boldsymbol{\omega}_i$ is nonzero only over E and E', and equation (8) becomes

$$\sum_{j=1}^{4} B_{E,ij}\, Q_{\partial E,j} + \sum_{j=1}^{4} B_{\partial E',ij}\, Q_{\partial E',j} = h_E - h_{E'}, \tag{9}$$

where $Q_{\partial E,j}$ ($j = 1 \ldots 4$) are local fluxes at the edges of the element E. Links between local and global numbering are based on the convention of Figure 1. For example, in the case depicted by Figure 2, the flux Q_i of the global numbering represents local fluxes $Q_{\partial E,1}$ and $Q_{\partial E',2}$. A local matrix $\mathbf{B}_E = [B_{E,ij}]$ of dimension 4×4 is introduced in (9) and defined by

$$B_{E,ij} = \int_E \left(\mathbf{K}_E^{-1}\, \boldsymbol{\omega}_j\right)\boldsymbol{\omega}_\iota, \tag{10}$$

where $\mathbf{K}_E$ is the tensor of hydraulic conductivity in E.

[20] By using local coordinates $x \in [0, \Delta x]$ and $y \in [0, \Delta y]$, the four local vector basis functions in the case of a rectangular element E can be written as

$$\begin{aligned}
\boldsymbol{\omega}_{E,1} &= \frac{1}{\Delta x \Delta y}\begin{pmatrix} x \\ 0 \end{pmatrix},\\
\boldsymbol{\omega}_{E,2} &= \frac{1}{\Delta x \Delta y}\begin{pmatrix} \Delta x - x \\ 0 \end{pmatrix},\\
\boldsymbol{\omega}_{E,3} &= \frac{1}{\Delta x \Delta y}\begin{pmatrix} 0 \\ y \end{pmatrix},\\
\boldsymbol{\omega}_{E,4} &= \frac{1}{\Delta x \Delta y}\begin{pmatrix} 0 \\ \Delta y - y \end{pmatrix}.
\end{aligned} \tag{11}$$

Considering here for the sake of simplicity that $\mathbf{K}_E = \begin{bmatrix} K_{E,x} & 0 \\ 0 & K_{E,y} \end{bmatrix}$, the local matrix $\mathbf{B}_E$ can be evaluated exactly:

$$\mathbf{B}_E = \frac{1}{6}\begin{pmatrix} 2\varsigma_{E,x} & \varsigma_{E,x} & 0 & 0 \\ \varsigma_{E,x} & 2\varsigma_{E,x} & 0 & 0 \\ 0 & 0 & 2\varsigma_{E,y} & \varsigma_{E,y} \\ 0 & 0 & \varsigma_{E,y} & 2\varsigma_{E,y} \end{pmatrix}, \tag{12}$$

where $\varsigma_{E,x} = (1/K_{E,x})(\Delta x/\Delta y)$ and $\varsigma_{E,y} = (1/K_{E,y})(\Delta y/\Delta x)$. For the elliptic case ($c = 0$), and by using Γ_E as test functions, the variational formulation of the mass conservation equation (1) gives (remember that $\Gamma_E = 1$ over E and 0 elsewhere)

$$\begin{aligned}
\int_\Omega \nabla \mathbf{q}\, \Gamma_E &= \sum_{i=1}^{\mathrm{Ned}} Q_i \int_\Omega (\nabla\, \boldsymbol{\omega}_i)\, \Gamma_E = \sum_{j=1}^{4} Q_{\partial E,j} \int_E \nabla \boldsymbol{\omega}_{E,j}\\
&= \int_\Omega f\, \Gamma_E = Q_{E,S},
\end{aligned} \tag{13}$$

where $Q_{E,S}$ is the sink/source term over the element E. According to (11), equation (13) yields

$$Q_{\partial E,1} - Q_{\partial E,2} + Q_{\partial E,3} - Q_{\partial E,4} = Q_{E,S}. \tag{14}$$

Neumann boundary conditions are added at this level; if a prescribed flux is assigned to the edge i of E, the corresponding flux $Q_{\partial E,i}$ is replaced by the prescribed value.

2.1.3. Final System

[21] The final system with the standard MFE is given by writing equation (9) for all interior and Dirichlet edges and equation (14) for all elements. With fluxes across edges and pressure head at elements as unknowns, the system has the following form:

$$\begin{pmatrix} \mathbf{M}_B & -\mathbf{M}_A^T \\ \mathbf{M}_A & 0 \end{pmatrix}\begin{pmatrix} \mathbf{Q} \\ \mathbf{h} \end{pmatrix} = \begin{pmatrix} \mathbf{R}^h \\ \mathbf{R}^Q \end{pmatrix}, \tag{15}$$

where $\mathbf{Q}$ and $\mathbf{h}$ are vectors of flux and head unknowns, respectively. $\mathbf{R}^h$ (enclosing Dirichlet boundary conditions) and $\mathbf{R}^Q$ (enclosing sink-source terms and Neumann boundary conditions) are the so-called residual vectors of Darcy's and mass balance equations.

[22] The linear system (15) involves a large number of unknowns (Ne + Ned). In addition, for steady state conditions, the system (15) is symmetric but not positive definite, which makes it difficult to handle with powerful iterative solvers based on conjugate gradients [*Golub and Van Loan*, 1989; *Brezzi and Fortin*, 1991; *Bergamaschi and Putti*, 1999].

[23] An improvement can be made provided that $\mathbf{M}_B$ is easily inverted. In this case, $\mathbf{Q}$ can be eliminated from (15), and a positive definite system, also called the Schur complement form, is written as

$$\mathbf{M}_A \mathbf{M}_B^{-1} \mathbf{M}_A^T \mathbf{h} = \mathbf{R}^Q - \mathbf{M}_A \mathbf{M}_B^{-1} \mathbf{R}^h. \tag{16}$$

[24] This equation is advantageous in that it both reduces the number of calculated unknowns and turns the indefinite system (15) into a symmetric and positive definite system (16). The main difficulty is that in general, $\mathbf{M}_B^{-1}$ is not computable (from a practical point of view) in an explicit way [*Brezzi et al.*, 2004]. Several techniques have been proposed in the literature to overcome this problem of poorly conditioned systems resulting from MFEs. Among theses approaches, the hybrid [*Roberts and Thomas*, 1989], the Uzawa [*Quarteroni and Valli*, 1994; *Bergamaschi et al.*, 1994], and the augmented Lagrangian [*Glowinski and Le Tallec*, 1989] techniques can be pointed out. The Uzawa method can be hampered by the large memory requirements of the algebraic solver, and the convergence properties of the augmented Lagrangian method strongly depend on a penalization parameter, whose optimal value may be difficult to evaluate [*Bergamaschi et al.*, 1994]. Note that *Aarnes et al.* [2005] obtained a system similar to (15) with the mixed multiscale finite element method that they solve via a

reduction to three symmetric and positive definite systems. *Powell* [2005] solved the indefinite system (15) by using the Krylov subspace minimal residual (MINRES) method [*Paige and Saunders*, 1975] with a suitable block-diagonal preconditioner and multigrid techniques [*Arnold et al.*, 1997]. Finally, the so-called hybrid technique remains the most widely used approach. It allows us to seek the solution of a symmetric positive definite system with a smaller number of unknowns than the original system (15).

2.2. Mixed Hybrid Finite Element Method for General Grids

[25] The idea of hybridization was raised and first used by *Fraeijs de Veubeke and Hugge* [1972] in order to simplify the linear system (15) resulting from the conventional MFEs. A first request for hybridization is to make the vector basis functions of the velocity interpolation nonnull only inside a single element E. The fluxes are counted positive outward. For example, the RT0 vectors of rectangles given in expression (6) become

$$\boldsymbol{\omega}_i = \begin{cases} \boldsymbol{\omega}_i = \dfrac{1}{|E|}\begin{pmatrix} x - x_{i-1} \\ 0 \end{pmatrix} & \text{on } E \\ 0 & \text{elsewhere.} \end{cases} \tag{17}$$

Therefore, all integrals reduce from the whole domain Ω to the element level E since both velocity and pressure head are approximated with basis functions that are nonzero inside the element E only.

[26] Then, new variables corresponding to the pressure head at the edges of an element are defined, and the fluxes are indirectly coupled by an explicit extra set of constraints (continuity of fluxes and heads along interfaces between elements). The hybrid formulation leads to a symmetric positive definite system with a smaller number of unknowns than the original problem. The principal stages of hybridization for both RT0 and BDM1 are detailed in sections 2.2.1–2.2.3 for general triangular and quadrangular shaped meshes.

2.2.1. Approximation Spaces

[27] For general triangular and quadrangular grids, vector basis functions are defined over a reference element $\hat{E}$ which can be transformed and exported toward the physical space (and real grid) by mapping. The mapping $F = F_E : \hat{E} \rightarrow E$ is linear for any triangular element E but nonlinear for any quadrangular element E. The mapping is detailed in Appendix A for both cases. Note that vectors are transformed from the reference space to the physical one via the Piola transform [*Brezzi and Fortin*, 1991]; namely, the vector basis function in the physical space $\boldsymbol{\omega}_{E,i}^{\mathrm{RT0}}$ is related to the vector basis function $\hat{\boldsymbol{\omega}}_i^{\mathrm{RT0}}$ in the reference space by

$$\boldsymbol{\omega}_{E,i}^{\mathrm{RT0}} = \frac{1}{\det(\mathbf{J})}\mathbf{J}\hat{\boldsymbol{\omega}}_{E,i}^{\mathrm{RT0}}, \tag{18}$$

where $\mathbf{J}$ is the Jacobian matrix (with components $\partial x_i/\partial \hat{x}_j$) and $\det(\mathbf{J})$ is its determinant. This transformation preserves normal components, i.e., fluxes (see *Brezzi and Fortin* [1991] for details):

$$Q_{\partial E,i} = \int_{\partial E_i} \mathbf{q}\mathbf{n}_{E_i} = \int_{\widehat{\partial E_i}} \widehat{\mathbf{q}}\widehat{\mathbf{n}}_{\partial E_i}, \tag{19}$$

where $\mathbf{n}_{\partial E_i}$ is the unit outward normal vector, which implies that $Q_{\partial E,i}$ is positive for outflow.

2.2.1.1. Lowest-Order Raviart-Thomas Space

[28] With RT0, pressure heads and fluxes are constant along the edge of an element. The velocity $\mathbf{q}$ over E is approximated by

$$\mathbf{q}_E = \sum_{i=1}^{\mathrm{Ned}_E} Q_{\partial E,i}\boldsymbol{\omega}_{E,i}^{\mathrm{RT0}}, \tag{20}$$

where $\boldsymbol{\omega}_{E,i}^{\mathrm{RT0}}$ is the RT0 basis function, $Q_{\partial E,i}$ is the flux through the edge i assumed to be constant along the edge, and Ned_E is the number of edges of E. The vector basis functions are defined in the reference element and have the following general form (see Figure 3 for the local numbering):

$$\widehat{\boldsymbol{\omega}}_{E,i}^{\mathrm{RT0}} = \begin{pmatrix} a_i^{\mathrm{RT0}} + b_i^{\mathrm{RT0}}\hat{x} \\ c_i^{\mathrm{RT0}} + d_i^{\mathrm{RT0}}\hat{y} \end{pmatrix} \text{ for } i = 1, \ldots, \mathrm{Ned}_E, \tag{21}$$

where $\hat{x}$ and $\hat{y}$ are the coordinates on the reference element and Ned_E is the number of edges. For a triangular element, we also have $d_i^{\mathrm{RT0}} = b_i^{\mathrm{RT0}}$.

[29] The constants a_i^{RT0}, b_i^{RT0}, c_i^{RT0}, and d_i^{RT0} in (21) are obtained by using a property of the vector basis functions stating that for each edge k of E with a unit outward normal vector $\mathbf{n}_{\partial E_k}$, we have

$$\int_{\partial E_k} \widehat{\boldsymbol{\omega}}_{E,i}^{\mathrm{RT0}} \cdot n_{\partial E_k} = \delta_{ik} \text{ for } k = 1, \ldots, \mathrm{Ned}_E. \tag{22}$$

The analytical expressions of these functions and Figure B1, which sketches their value within the element E, are provided in Appendix B.

2.2.1.2. Brezzi-Douglas-Marini Space of First Order

[30] With BDM1, it is postulated that the normal velocity may vary linearly along each edge. Therefore, the velocity inside the element is approximated by

$$\mathbf{q}_E = \sum_{i=1}^{\mathrm{Ned}_E}\sum_{j=1}^{2} Q_{\partial E,i,j}\boldsymbol{\omega}_{E,i,j}^{\mathrm{BDM1}}, \tag{23}$$

where edges are indexed by i and the additional index j (j = 1, 2) denotes the two degrees of freedom $Q_{\partial E,i,j}$ per edge needed to describe the linear variation of the flux along the edge. Generally, these degrees of freedom are the zero and the first moments of the normal velocity along each edge i of E. They are defined by $(1/|\partial E_i|)\int_{\partial E_i} \mathbf{q}_E \cdot \mathbf{n}_{\partial E_i} \mathrm{d}\ell$ and $(1/|\partial E_i|)\int_{\partial E_i} \mathbf{q}_E \cdot \mathbf{n}_{\partial E_i} \ell \mathrm{d}\ell$, where $|\partial E_i|$ represents the length of the edge ∂E_i [*Beckie et al.*, 1993; *Bergamaschi*

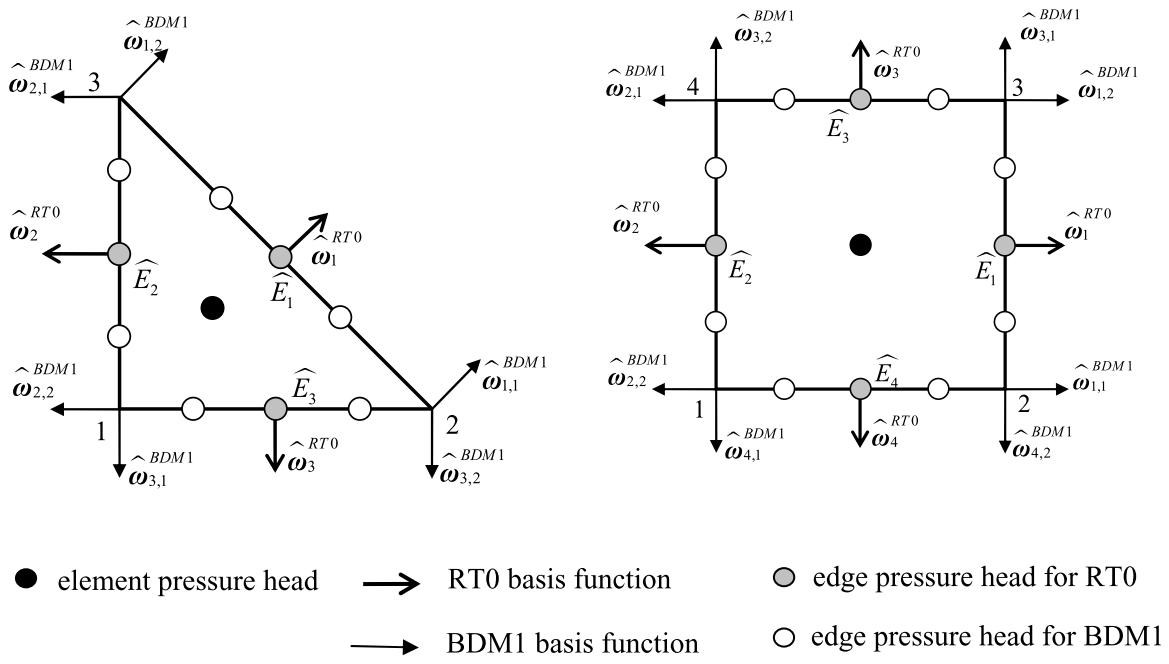

Figure 3. Definition of the unknowns and indexes of edges, vertices, and basis functions. For RT0 basis functions, flux and head values are averaged over the edge. For BDM1 functions, flux and head values correspond to local point values.

et al., 1994]. These degrees of freedom can also be the values of $\mathbf{q}_E \cdot \mathbf{n}_{\partial E_i}$ at two different points located anywhere on the edge. In this work, as in the works by *Wheeler and Yotov* [2006a] or *Brezzi et al.* [2004], the locations of these two points are chosen at the end points of the edge (see Figure 3).

[31] For a triangular element, the vector basis functions in the reference element have the following form:

$$\widehat{\boldsymbol{\omega}}_{E,i,j}^{\mathrm{BDM1}} = \begin{pmatrix} a_{i,j}^{\mathrm{BDM1}} + b_{i,j}^{\mathrm{BDM1}}\hat{x} + c_{i,j}^{\mathrm{BDM1}}\hat{y} \\ \\ d_{i,j}^{\mathrm{BDM1}} + e_{i,j}^{\mathrm{BDM1}}\hat{x} + f_{i,j}^{\mathrm{BDM1}}\hat{y} \end{pmatrix} \quad \text{for } i = 1,\ldots,3 \text{ and } j = 1,\ldots,2, \tag{24}$$

whereas these basis functions in a quadrangular element are written as

$$\widehat{\boldsymbol{\omega}}_{E,i,j}^{\mathrm{BDM1}} = \begin{pmatrix} a_{i,j}^{\mathrm{BDM1}} + b_{i,j}^{\mathrm{BDM1}}\hat{x} + c_{i,j}^{\mathrm{BDM1}}\hat{y} + d_{i,j}^{\mathrm{BDM1}}\hat{x}^2 + 2e_{i,j}^{\mathrm{BDM1}}\hat{x}\hat{y} \\ f_{i,j}^{\mathrm{BDM1}} + g_{i,j}^{\mathrm{BDM1}}\hat{x} + h_{i,j}^{\mathrm{BDM1}}\hat{y} - 2d_{i,j}^{\mathrm{BDM1}}\hat{x}\hat{y} - e_{i,j}^{\mathrm{BDM1}}\hat{y}^2 \end{pmatrix} \quad \text{for } i = 1,\ldots,4 \text{ and } j = 1,\ldots,2. \tag{25}$$

The scalar coefficients in (24) and (25) are obtained by writing

$$\widehat{\boldsymbol{\omega}}_{E,i,j}^{\mathrm{BDM1}}(r_{lk})\mathbf{n}_{\partial E_l} = \frac{2}{|\partial E_l|}\delta_{il}\delta_{jk} \text{ for } l = 1,\ldots,\mathrm{Ned}_E \text{ and } k = 1,2. \tag{26}$$

The meaning of (26) is that for a given $\widehat{\boldsymbol{\omega}}_{E,i,j}^{\mathrm{BDM1}}$, for all edges l of E formed by the two end points r_{lk} (k = 1, 2), and for a normal vector $\mathbf{n}_{\partial E_l}$, the value of $\widehat{\boldsymbol{\omega}}_{E,i,j}^{\mathrm{BDM1}}\,\mathbf{n}_{E_l}$ at the point r_{lk} is nonnull only if $l = i$ and $k = j$. The analytical expressions of these functions and Figure B1, which sketches their value within the element E, are reported in Appendix B.

2.2.2. Discretization With the MHFE Formulation

[32] For RT0, the head is assumed constant along the edge, denoted $Th_{\partial E,i}$, and corresponds to the average head value on the edge i of E. For BDM1, the head is linear along the edge, with two degrees of freedom, $Th\partial_{E,i,1}$ and $Th_{\partial E,i,2}$, corresponding to head values at two points of the edge i (these points are not necessarily the same as that for fluxes across the edge). Since the mathematical developments are quite similar for both basis functions RT0 and BDM1 ($\boldsymbol{\omega}_{E,i}^{\mathrm{RT0}}$ is replaced by $\boldsymbol{\omega}_{E,i,j}^{\mathrm{BDM1}}$), the hybridization is only detailed below for RT0 functions.

[33] The variational formulation of Darcy's law ($\mathbf{K}^{-1}\mathbf{q} = -\nabla h$) is written by using the vector basis functions $\boldsymbol{\omega}_{E,i}^{\mathrm{RT0}}$ as test functions:

$$\int_E \mathbf{K}^{-1}\mathbf{q}_E\boldsymbol{\omega}_{E,i}^{\mathrm{RT0}} = -\int_E \nabla h\boldsymbol{\omega}_{E,i}^{\mathrm{RT0}} = \int_E h\,\nabla\boldsymbol{\omega}_{E,i}^{\mathrm{RT0}} - \sum_{k=1}^{\mathrm{Ned}_E}\int_{\partial E_k} h\boldsymbol{\omega}_{E,i}^{\mathrm{RT0}}\mathbf{n}_{\partial E_k}. \tag{27}$$

Using property (22) of the basis functions allows us to rewrite (27) as

$$\int_E \mathbf{K}^{-1}\mathbf{q}_E\boldsymbol{\omega}_{E,i}^{\mathrm{RT0}} = h_E - Th_{\partial E,i}, \tag{28}$$

where h_E is the average head in the element and $Th_{\partial E,i}$ is the average head on edge ∂E_i. Using the approximation (20) for the velocity over the element E leads to

$$\sum_{k=1}^{\mathrm{Ned}_E} B_{E,i,k} Q_{\partial E,k} = h_E - Th_{\partial E,i}, \tag{29}$$

where the elemental matrix $\mathbf{B}_E = [B_{E,i,k}]$ of dimension $\mathrm{Ned}_E \times \mathrm{Ned}_E$ is defined by

$$B_{E,i,k} = \int_E \boldsymbol{\omega}_{E,i}^{\mathrm{RT0},T} \mathbf{K}^{-1} \boldsymbol{\omega}_{E,k}^{\mathrm{RT0}}. \tag{30}$$

This matrix $\mathbf{B}_E$ is symmetric and positive definite. Equation (29) can be rewritten to express each flux through edge ∂E_i as

$$Q_{\partial E,i} = \sum_{k=1}^{\mathrm{Ned}_E} B_{E,i,k}^{-1} \left(h_E - Th_{\partial E,k}\right). \tag{31}$$

[34] The mass balance equation (1) is discretized by using a finite volume formulation in space and a first-order finite difference in time:

$$c_E |E| \frac{h_E^{n+1} - h_E^n}{\Delta t} + \sum_{i=1}^{\mathrm{Ned}_E} Q_{\partial E,i} = |E| f_E = Q_{E,s}, \tag{32}$$

where c_E and f_E are the mean values over the element E of the storage coefficient c and the sink/source term f, respectively. Combining (31) and (32) yields

$$h_E^{n+1} = \sum_{i=1}^{\mathrm{Ned}_E} \frac{\alpha_{E,i}}{\beta_E} Th_{\partial E,i}^{n+1} + \frac{\lambda_E}{\beta_E} h_E^n + \frac{Q_{E,s}}{\beta_E}, \tag{33}$$

where $\lambda_E = \frac{c_E |E|}{\Delta t}$, $\alpha_{E,i} = \sum_{j=1}^{\mathrm{Ned}_E} B_{E,ij}^{-1}$, $\alpha_E = \sum_{i=1}^{\mathrm{Ned}_E} \alpha_{E,i}$, and $\beta_E = (\lambda_E + \alpha_E)$.

[35] Finally, the expression of fluxes through the edges of the element E is obtained by substituting (33) in (31), yielding

$$Q_{\partial E,i}^{n+1} = \sum_{j=1}^{\mathrm{Ned}_E} N_{E,ij} Th_{\partial E,j}^{n+1} + F_{E,i}^n, \tag{34}$$

where

$$N_{E,ij} = \frac{\alpha_{E,i}\alpha_{E,j}}{\beta_E} - B_{E,ij}^{-1}, \tag{35}$$

$$F_{E,i}^n = \lambda_E \frac{\alpha_{E,i}}{\beta_E} h_E^n + \frac{\alpha_{E,i}}{\beta_E} Q_{E,s}. \tag{36}$$

Equation (34) is used to form the final system of equations handling the mean pressure head on edges as scalar unknowns ($Th_{\partial E,i}$, $i = 1, \ldots, Nf$, where Nf is the total number of edges in the meshing of the domain minus the number of edges assigned to Dirichlet boundary conditions). This final system is built by using continuity properties for all interior edges. The continuity of both the head and the normal component of velocity at the edge between two adjacent elements E and E' is written as

$$\begin{aligned} Th_{\partial E,i} &= Th_{\partial E',j}, \\ Q_{\partial E,i} + Q_{\partial E',j} &= 0, \end{aligned} \tag{37}$$

where i and j are the local numbering of the same edge. The fluxes in equation (37) are replaced by their expression in (34), which leads to an equation with $Th_{\partial E,i}$ as unknowns. Boundary conditions are handled as follows. For an edge with a Dirichlet condition, i.e., an edge ∂E_i with a prescribed head Th_i^D,

$$Th_{\partial E,i} = Th_i^D. \tag{38}$$

For an edge ∂E_i with a Neumann boundary condition, it is stated that

$$Q_{\partial E,i} = Q_i^N, \tag{39}$$

where Q_i^N is counted positive for outflow.

[36] In the case of BDM1 approximation, the local head and flux along each edge evolve linearly. If the two degrees of freedom for head, $Th_{\partial E,i,1}$ and $Th_{\partial E,i,2}$, are chosen at points located at one third and two thirds of the edge length, the variational formulation of Darcy's law is written as

$$\begin{aligned} \int_E \mathbf{K}^{-1} \mathbf{q}_E \boldsymbol{\omega}_{E,i,j}^{\mathrm{BDM1}} &= -\int_E \nabla h \boldsymbol{\omega}_{E,i,j}^{\mathrm{BDM1}} \\ &= \int_E h \nabla \boldsymbol{\omega}_{E,i,j}^{\mathrm{BDM1}} - \sum_{k=1}^{\mathrm{Ned}_E} \int_{\partial E_k} h \boldsymbol{\omega}_{E,i,j}^{\mathrm{BDM1}} \mathbf{n}_{\partial E_k} \\ &= h_E - Th_{\partial E,i,j}. \end{aligned} \tag{40}$$

[37] The further developments are similar to those of RT0 functions with a velocity $\mathbf{q}_E$ interpolated by using values $Q_{\partial E,i,1}$ and $Q_{\partial E,i,2}$ as seeds located at end points of each edge ∂E_i (see Figure 3). The elemental matrix $\mathbf{B}_E = [B_{E,i,j,k,l}]$ is of dimension ($2\mathrm{Ned}_E \times 2\mathrm{Ned}_E$) with components in the form

$$B_{E,i,j,k,l} = \int_E \boldsymbol{\omega}_{E,i,j}^{\mathrm{BDM1},T} \mathbf{K}^{-1} \boldsymbol{\omega}_{E,k,l}^{\mathrm{BDM1}}. \tag{41}$$

2.2.3. Some General Remarks

[38] 1. In the previous developments, the sole requested local calculation is that of integrals enclosed in the local matrix $\mathbf{B}_E$ (30) or (41). Most often, these integrals cannot be evaluated in the real element, which forces us to resort to the reference element by using the following transform:

$$B_{E,i,k} = \int_{\hat{E}} \widehat{\boldsymbol{\omega}}_i^{\mathrm{RT0},T} \widehat{K}^{-1} \widehat{\boldsymbol{\omega}}_k^{\mathrm{RT0}}, \tag{42}$$

where $\widehat{\mathbf{K}}^{-1} = \mathbf{J}^T \mathbf{K}^{-1} \mathbf{J} / |\mathbf{J}|$ corresponds to the analog tensor in the reference element [*Marsden and Hughes*,

1983]. The same transformation also applies to the BDM1 formulation (41).

[39] 2. The matrix $\mathbf{B}_E$ (30) and therefore the matrix $\mathbf{N}_E$ (35) cannot be evaluated analytically for general quadrangles and requires numerical integration. The matrix components are evaluated on a square-shaped reference element by means of quadrature formulas. However, this procedure may affect the quality of the results, especially for distorted meshes and highly anisotropic domains [*Younes and Fontaine*, 2008a]. On the other hand, for parallelograms and triangular elements, the Piola transform (18) is affine, and the determinant of the Jacobian matrix is constant (it does not depend on the coordinates of the reference space), allowing the matrix $\mathbf{N}_E$ to be evaluated analytically.

[40] 3. The size of the system for the RT0 hybrid formulation is equal to the total number of edges excluding Dirichlet boundaries. The stiffness matrix is symmetric, positive definite, with a structure of $(2\ \mathrm{Ned}_E - 1)$-point stencil. The BDM1 hybrid formulation leads to a system of size twice the total number of edges inside the domain plus twice the number of edges with Neumann conditions. The matrix is also symmetric, positive definite, but with a stencil of $2(2\ \mathrm{Ned}_E - 1)$.

3. REDUCING THE NUMBER OF UNKNOWNS BY ALTERNATIVE FORMULATIONS AND APPROXIMATIONS

3.1. Diagonal Tensor Coefficient

[41] As shown in section 2, the standard RT0 MFE method requires a lot of unknowns, i.e., the number of edges (for fluxes) plus the number of elements (for the pressure head). The hybridization technique reduces the size of the problem down to, roughly, the number of edges. Many authors tried to improve this reduction and, in this process, to find formal links between MFE or MHFE and finite volume methods [e.g., *Russell and Wheeler*, 1983; *Baranger et al.*, 1994; *Arbogast et al.*, 1997; *Younes et al.*, 1999b; *Cai et al.*, 2003].

[42] The first attempts were all based on quadrature formula to make the elemental matrix $\mathbf{B}_E$ diagonal in order to obtain a final system with the cell pressure heads as unknowns. For rectangular meshes and a diagonal tensor $\mathbf{K}$, the RT0 MFE can be reduced to standard cell-centered finite differences [*Russell and Wheeler*, 1983; *Weiser and Wheeler*, 1988; *Chavent and Roberts*, 1991]. The basic idea is to handle the integrals by using the following quadrature expression for any function $\varphi\ (x, y)$ over an element E:

$$\int_E \varphi(x,y) = \frac{|E|}{4}\sum_{i=1}^{4}\varphi(x_i,y_i), \tag{43}$$

where (x_i, y_i) are the coordinates of the vertices and $|E|$ is the area of the element E.

[43] By using (43) to evaluate $B_{E,ij} = \int_E (\mathbf{K}_E^{-1}\ \boldsymbol{\omega}_j)\boldsymbol{\omega}_\iota$ with $K_E = \begin{bmatrix} K_{E,x} & 0 \\ 0 & K_{E,y} \end{bmatrix}$ and the vector basis functions given in (11), the matrix B_E defined by (10) becomes

$$\mathbf{B}_E = \frac{1}{2}\begin{pmatrix} \varsigma_{E,x} & 0 & 0 & 0 \\ 0 & \varsigma_{E,x} & 0 & 0 \\ 0 & 0 & \varsigma_{E,y} & 0 \\ 0 & 0 & 0 & \varsigma_{E,y} \end{pmatrix}, \tag{44}$$

where $\varsigma_{E,x} = (1/K_{E,x})(\Delta x/\Delta y)$ and $\varsigma_{E,y} = (1/K_{E,y})(\Delta y/\Delta x)$. For instance, the expression (9) for a vertical edge such as that in Figure 2 is rewritten as

$$Q_{\partial E,i} = 2\frac{h_E - h_{E'}}{\varsigma_{E,x} + \varsigma_{E',x}}, \tag{45}$$

yielding in the case of uniform discretization over the whole domain (at steps Δx and Δy)

$$Q_{\partial E,i} = \Delta y \frac{2}{\dfrac{1}{K_{E,x}} + \dfrac{1}{K_{E',x}}}\frac{h_E - h_{E'}}{\Delta x}. \tag{46}$$

This equation shows that the mixed approach reduces to the standard finite difference method with the so-called interblock hydraulic conductivity corresponding to the harmonic mean between values of two adjacent elements E and E'.

[44] Then, equation (46) can be substituted in the discrete mass balance equation (32) to obtain the final system where unknowns are now the cell pressure heads. The stencil of the matrix is five in two dimensions, and the same technique applied to 3-D problems would yield a seven-point stencil [*Russell and Wheeler*, 1983]. This procedure was extended to triangular meshes by *Baranger et al.* [1994] and *Arbogast and Kennan* [1984], but the numerical diagonalization of the elemental matrix $\mathbf{B}_E$ seems accurate enough only for triangles with three sharp angles (all angles $<\pi/2$).

3.2. Full Tensor Coefficient

[45] A similar approach with a full tensor of hydraulic conductivity was formulated, analyzed, and tested by *Arbogast et al.* [1997]. Consider the elliptic form of the problem ($c = 0$ in equation (1)) over a rectangular meshing with a full tensor of conductivity $\mathbf{K} = \begin{bmatrix} K_{E,x} & K_{E,xy} \\ K_{E,xy} & K_{E,y} \end{bmatrix}$. A new variable $\mathbf{v}^e = -\nabla h$ is introduced and considered in RT0. Its variational form using $\boldsymbol{\omega}_i$ as test functions gives

$$\int_\Omega \mathbf{v}^e\boldsymbol{\omega}_i + \int_\Omega \nabla h\,\boldsymbol{\omega}_i = 0. \tag{47}$$

In the case of an edge i inside the domain and shared by the adjacent elements E and E', this form leads to (see equation (9) for comparison purposes)

$$\sum_{j=1}^{4} B_{E,i,j}\,V^e_{\partial E,j} + \sum_{j=1}^{4} B_{E',i,j}\,V^e_{\partial E',j} = h_E - h_{E'}. \tag{48}$$

[46] Using the trapezoidal rule (43) for the integration (as done previously in (45)) gives for a vertical edge

$$V^e_{\partial E,i} = 2\Delta y \frac{h_E - h_{E'}}{\Delta x|_E + \Delta x|_{E'}}. \quad (49)$$

The variational formulation of the velocity $\mathbf{q} = \mathbf{K}\mathbf{v}^e$ is also used:

$$\int_\Omega \mathbf{q}\,\omega_i = \int_\Omega \mathbf{K}\mathbf{v}^e \omega_i, \quad (50)$$

which can be rewritten as

$$\sum_{j=1}^{4} B_{E,ij}\, Q_{\partial E,j} + \sum_{j=1}^{4} B_{E',ij}\, Q_{\partial E',j} = \sum_{j=1}^{4} B^e_{E,ij}\, V^e_{\partial E,j} + \sum_{j=1}^{4} B^e_{E',ij}\, V^e_{\partial E',j}. \quad (51)$$

[47] Again, the trapezoidal rule is applied to calculate the terms of the local matrix $\mathbf{B}_E$. For the vertical edge ∂E_i between the elements E and E', the left-hand side of (51) becomes

$$\sum_{j=1}^{4} B_{E,ij}\, Q_{\partial E,j} + \sum_{j=1}^{4} B_{E',ij}\, Q_{\partial E',j} = \frac{1}{2\Delta y}\left(\Delta x|_E + \Delta x|_{E'}\right) Q_{\partial E,i}. \quad (52)$$

All calculations done, the first term in the right-hand side of (51) gives

$$\sum_{j=1}^{4} B^e_{E,ij}\, V^e_{\partial E,j} = \frac{\Delta x|_E}{4\Delta y}\left[K_{E,x}\big|_{\Delta x,0} + K_{E,x}\big|_{\Delta x,\Delta y}\right] V^e_{\partial E,1} + \left[\frac{1}{4} K_{E,x}\Big|_{\Delta x,\Delta y}\right] V^e_{\partial E,3} + \left[\frac{1}{4} K_{E,x}\Big|_{\Delta x,0}\right] V^e_{\partial E,4}, \quad (53)$$

and similarly, the second term in the right-hand side of (51) is written as

$$\sum_{j=1}^{4} B^e_{E',ij}\, V^e_{\partial E',j} = \frac{\Delta x|_{E'}}{4\Delta y}\left[K_{E',x}\big|_{0,0} + K_{E',x}\big|_{0,\Delta y}\right] V^e_{\partial E',2} + \left[\frac{1}{4} K_{E',x}\Big|_{0,\Delta y}\right] V^e_{\partial E',3} + \left[\frac{1}{4} K_{E',x}\Big|_{0,0}\right] V^e_{\partial E',4}, \quad (54)$$

with $S|_{a,b}$ denoting the value taken by S at the point of local coordinates (a, b). Substituting (52), (53), and (54) in (51) and using the indexation reported in Figure 4 allows us to write

$$Q_i = \frac{\Delta y/2}{\Delta x|_E + \Delta x|_{E'}}\left\{\frac{\Delta x|_E}{\Delta y}\left(K_x|_{i,1} + K_x|_{i,2}\right) V^e_{\partial E,1} + K_x|_{i,2} V^e_{\partial E,3} + K_x|_{i,1} V^e_{\partial E,4} + \frac{\Delta x|_{E'}}{\Delta y}\left(K_x|_{i,1} + K_x|_{i,2}\right) V^e_{\partial E',2} + K_x|_{i,2} V^e_{\partial E',3} + K_x|_{i,1} V^e_{\partial E',4}\right\}. \quad (55)$$

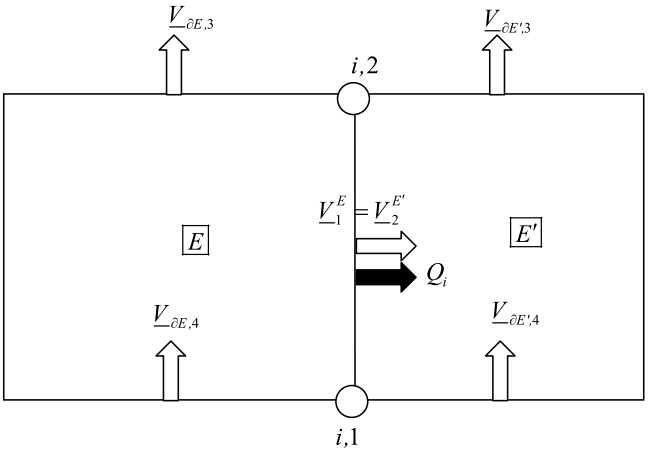

Figure 4. Indexation for the extended approach.

[48] Given the expressions of the head gradients $V^e_{\partial E,i}$ in (49) and by substituting (55) in mass balance equation (14), a symmetric nine-point scheme is obtained. This scheme is quite similar to the standard finite difference method for diffusion problems with a full tensor coefficient [e.g., *Zheng and Bennett*, 1995]. Note, however, that in general, the standard finite difference scheme does not yield a symmetric system matrix contrary to the present one [*Cirpka et al.*, 1999]. In essence, scheme (55) is also suited for cases in which the conductivity may locally tend to zero (contrary to the standard MFE approach, equation (55) does not contain the inverse of the conductivity tensor).

[49] The method was tentatively extended to more general quadrangular meshes by *Arbogast et al.* [1998]. Note that at nonsmooth grid interfaces, or at interfaces with discontinuity of conductivities, it is impossible to obtain continuous normal components for both q and $\mathbf{v}^e$. In this case, the method can suffer from severe loss of accuracy [*Klausen and Russell*, 2005]. To overcome this problem, the method has to introduce Lagrange multipliers at nonsmooth grid interfaces or at interfaces with a discontinuity of conductivities. This partial hybridization is named the enhanced cell centered finite difference method [*Arbogast et al.*, 1998; *Wheeler et al.*, 2002].

3.3. Reformulation by Using a New Variable on Triangles

[50] Almost 10 years ago, another approach to the MHFEs was developed for both the elliptic case [*Younes et al.*, 1999b] and the parabolic case [*Younes et al.*, 1999c] on triangles. The main idea motivating this approach was to reduce the number of unknowns from pressure head on edges to a single unknown per element. This unknown is not an average value like that of the standard finite volume approximation, and it can be located somewhere, inside or outside the element, according to the shape of the element and the type of manipulated PDE (parabolic or elliptic). This single-unknown scheme was also analyzed by *Chavent et al.*

[2003] with special care to singular elements and singular edges.

[51] In sections 3.3.1 and 3.3.2, the method is briefly described, and the equivalence between this RT0 approach with a single unknown per element and the MHFE method is shown. For the sake of simplicity, the developments are limited to steady state flow with a full tensor coefficient and sink/source terms.

3.3.1. RT0 MHFE Method for Elliptic Problems on Triangles

[52] In the case of a triangular element E, the vector basis functions RT0 $\omega_{E,i}$ of MHFE can be obtained in the physical space by using (18), which gives [*Kaasschieter and Huijben*, 1992]

$$\omega_{E,i} = \frac{1}{2|E|}\begin{pmatrix} x - x_i \\ y - y_i \end{pmatrix}, \tag{56}$$

where (x_i, y_i) are the coordinates of the vertex opposite to the edge i. Let $\mathbf{x}_{ij}$ denote the edge vector from node i toward node j and l_{ij} be the scalar measure defined by

$$l_{ij} = \mathbf{x}_{ij}^T (\mathbf{K}_E)^{-1} \mathbf{x}_{ij}, \tag{57}$$

where $\mathbf{K}_E$ is the full tensor of conductivity.

The local matrix $\mathbf{B}_E$ defined by equation (30) can be evaluated analytically, leading to

$$\mathbf{B}_E = \frac{1}{48|E|} \cdot \begin{pmatrix} 3l_{12} + 3l_{13} - l_{23} & -3l_{12} + l_{13} + l_{23} & l_{12} - 3l_{13} + l_{23} \\ -3l_{12} + l_{13} + l_{23} & 3l_{12} - l_{13} + 3l_{23} & l_{12} + l_{13} - 3l_{23} \\ l_{12} - 3l_{13} + l_{23} & l_{12} + l_{13} - 3l_{23} & -l_{12} + 3l_{13} + 3l_{23} \end{pmatrix}. \tag{58}$$

The following property can be noted:

$$\sum_{j=1}^{3} B_{E,ij} = \frac{1}{48|E|}(l_{12} + l_{13} + l_{23}) = L_E \tag{59}$$

for all i, where L_E is viewed as the inverse of the conductivity tensor scaled by the shape of the element. By using (59), the fluxes in (34) for the steady state case become

$$\begin{bmatrix} Q_{\partial E,1} \\ Q_{\partial E,2} \\ Q_{\partial E,3} \end{bmatrix} = \frac{1}{3}\mathbf{B}_E^{-1} \left(\begin{bmatrix} -2 & 1 & 1 \\ 1 & -2 & 1 \\ 1 & 1 & -2 \end{bmatrix} \begin{bmatrix} Th_{\partial E,1} \\ Th_{\partial E,2} \\ Th_{\partial E,3} \end{bmatrix} + L_E Q_{E,s} \begin{bmatrix} 1 \\ 1 \\ 1 \end{bmatrix} \right). \tag{60}$$

The inverse of the matrix $\mathbf{B}_E$ is obtained algebraically [*Younes et al.*, 2004]:

$$[\mathbf{B}_E]^{-1} = \frac{\det(\mathbf{K}_E)}{|E|} \begin{bmatrix} \mathbf{x}_{23}\mathbf{K}_E^{-1}\mathbf{x}_{23} & \mathbf{x}_{23}\mathbf{K}_E^{-1}\mathbf{x}_{31} & \mathbf{x}_{23}\mathbf{K}_E^{-1}\mathbf{x}_{12} \\ \mathbf{x}_{23}\mathbf{K}_E^{-1}\mathbf{x}_{31} & \mathbf{x}_{31}\mathbf{K}_E^{-1}\mathbf{x}_{31} & \mathbf{x}_{12}\mathbf{K}_E^{-1}\mathbf{x}_{31} \\ \mathbf{x}_{23}\mathbf{K}_E^{-1}\mathbf{x}_{12} & \mathbf{x}_{12}\mathbf{K}_E^{-1}\mathbf{x}_{31} & \mathbf{x}_{12}\mathbf{K}_E^{-1}\mathbf{x}_{12} \end{bmatrix} + \frac{1}{3L_E}\begin{bmatrix} 1 & 1 & 1 \\ 1 & 1 & 1 \\ 1 & 1 & 1 \end{bmatrix}, \tag{61}$$

where det() is the determinant of the matrix. Substituting (61) in (60) gives the expressions of the fluxes through the edges as

$$Q_{\partial E,i} = -\frac{\det(\mathbf{K}_E)}{|E|} \cdot \left[\left(\mathbf{x}_{jk}^T \mathbf{K}_E^{-1} \mathbf{x}_{jk} \right) Th_{\partial E,i} + \left(\mathbf{x}_{jk}^T \mathbf{K}_E^{-1} \mathbf{x}_{ki} \right) Th_{\partial E,j} + \left(\mathbf{x}_{jk}^T \mathbf{K}_E^{-1} \mathbf{x}_{ij} \right) Th_{\partial E,k} \right] + \frac{Q_{E,s}}{3}, \tag{62}$$

where i, j, and k are all different.

3.3.2. Reformulation by Using a New Variable

[53] The purpose is to reduce the size of this system by defining a new variable H_E associated with the element E by the following expression:

$$H_E = \sum_{i=1}^{3} \pi_{E,i} Th_{\partial E,i}. \tag{63}$$

In addition, H_E is such that the flux leaving E through the edge ∂E_i obeys the expression

$$Q_{\partial E,i} = \xi_{E,i}(H_E - Th_{\partial E,i}) + \gamma_{E,i}, \tag{64}$$

where $\pi_{E,i}$, $\xi_{E,i}$, and $\gamma_{E,i}$ are suited coefficients. Note that H_E is generally different from the mean pressure head h_E in the element given by (33). The coefficients $\pi_{E,i}$, $\xi_{E,i}$, and $\gamma_{E,i}$ are defined by substituting (63) into (64), and then the resulting expression is compared with the equation (62). Identification between both forms allows us to write

$$\pi_{E,i} = \frac{\det(\mathbf{K}_E)}{4|E|^2} \left[\mathbf{x}_{jk}^T \mathbf{K}_E^{-1} \mathbf{x}_{jk} \right] \left[\mathbf{x}_{ij}^T \mathbf{K}_E^{-1} \mathbf{x}_{kj} \right], \tag{65}$$

where i, j, and k are all different;

$$\xi_{E,i} = \frac{4|E|}{\left[\mathbf{x}_{ij}^T \mathbf{K}_E^{-1} \mathbf{x}_{ik} \right]}, \tag{66}$$

where i, j, and k are all different; and

$$\gamma_{E,1} = \gamma_{E,2} = \gamma_{E,3} = \frac{Q_{E,s}}{3}. \tag{67}$$

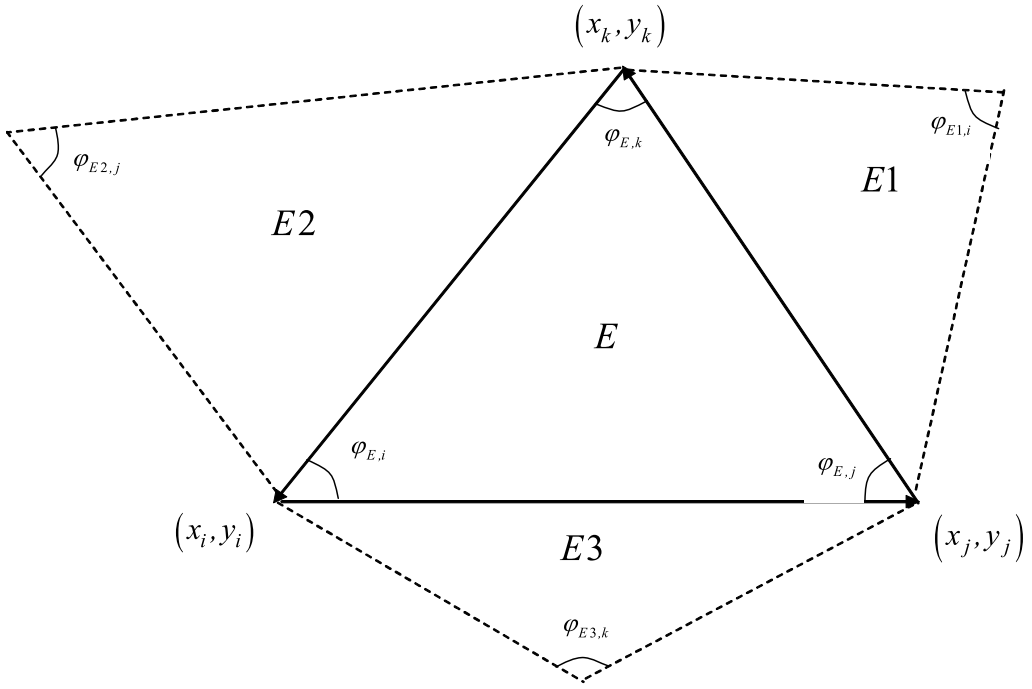

Figure 5. A triangular element with its three neighbors.

Substituting these relations in equation (63) leads to

$$H_E = \frac{\det(\mathbf{K}_E)}{4|E|^2}\Big[\left(\mathbf{x}_{ik}^T\mathbf{K}_E^{-1}\mathbf{x}_{jk}\right)\left(\mathbf{x}_{ij}^T\mathbf{K}_E^{-1}\mathbf{x}_{kj}\right)Th_{\partial E,i} + \left(\mathbf{x}_{ij}^T\mathbf{K}_E^{-1}\mathbf{x}_{ik}\right)\left(\mathbf{x}_{ik}^T\mathbf{K}_E^{-1}\mathbf{x}_{jk}\right)Th_{\partial E,j} + \left(\mathbf{x}_{ij}^T\mathbf{K}_E^{-1}\mathbf{x}_{ik}\right)\left(\mathbf{x}_{ij}^T\mathbf{K}_E^{-1}\mathbf{x}_{kj}\right)Th_{\partial E,k}\Big]. \quad (68)$$

[54] For the isotropic case ($K_{E,x} = K_{E,y} = K_E$ and $K_{E,xy} = 0$), H_E in (68) reduces to the simple linear interpolate of the three edge values $Th_{\partial E,j}$, $j = 1$, 2, and 3, at the circumcenter of the element E [*Cordes and Kinzelbach*, 1996; *Younes et al.*, 1999a]. As for classical MHFEs, the continuity of the pressure head and fluxes between two adjacent elements E and E' is obtained by substituting (64) in (37):

$$Q_{\partial E,i} = -Q_{\partial E',i} = \frac{\xi_{E,i}\xi_{E',i}}{\xi_{E,i} + \xi_{E',i}}[H_E - H_{E'}] - \frac{\xi_{E,i}}{\xi_{E,i} + \xi_{E',i}}\left[\gamma_{E,i} + \gamma_{E',i}\right] + \gamma_{E,i}. \quad (69)$$

[55] Introducing (69) in the steady state mass balance equation for the element E, i.e., $\sum_{i=1}^{3} Q_{\partial E,i} = Q_{E,s}$, surrounded by three elements $E1$, $E2$, and $E3$ (Figure 5) allows us to draw the following expression:

$$\frac{\xi_{E,i}\xi_{E1,i}}{\xi_{E,i} + \xi_{E1,i}}(H_E - H_{E1}) + \frac{\xi_{E,j}\xi_{E2,j}}{\xi_{E,j} + \xi_{E2,j}}(H_E - H_{E2}) + \frac{\xi_{E,k}\xi_{E3,k}}{\xi_{E,k} + \xi_{E3,k}}(H_E - H_{E3}) = \frac{\xi_{E,i}}{\xi_{E,i} + \xi_{E1,i}}\left(\gamma_{E,i} + \gamma_{E1,i}\right) + \frac{\xi_{E,j}}{\xi_{E,j} + \xi_{E2,j}}\left(\gamma_{E,j} + \gamma_{E2,j}\right) + \frac{\xi_{E,k}}{\xi_{E,k} + \xi_{E3,k}}\left(\gamma_{E,k} + \gamma_{E3,k}\right). \quad (70)$$

Basically, the system in (70) is positive definite provided that [*Chavent et al.*, 2003]

$$\left(\frac{\xi_{E,i}\xi_{E1,i}}{\xi_{E,i} + \xi_{E1,i}} + \frac{\xi_{E,j}\xi_{E2,j}}{\xi_{E,j} + \xi_{E2,j}} + \frac{\xi_{E,k}\xi_{E3,k}}{\xi_{E,k} + \xi_{E3,k}}\right) > 0. \quad (71)$$

[56] For the isotropic case, i.e., $K_{E,x} = K_{E,y} = K_E$ and $K_{E,xy} = 0$, for all elements E, the above condition becomes (see Figure 5 for notations)

$$\left(\frac{\cot\ \varphi_{E1,i}}{K_{E1}} + \frac{\cot\ \varphi_{E,i}}{K_E}\right)^{-1} + \left(\frac{\cot\ \varphi_{E2,j}}{K_{E2}} + \frac{\cot\ \varphi_{E,j}}{K_E}\right)^{-1} + \left(\frac{\cot\ \varphi_{E3,k}}{K_{E3}} + \frac{\cot\ \varphi_{E,k}}{K_E}\right)^{-1} > 0. \quad (72)$$

For homogeneous domains, expression (72) can be simplified by removing K, and the condition becomes equivalent to the Delaunay criterion [*Chavent et al.*, 2003].

[57] To sum up, the formulation of the MHFE method with a single unknown per triangular element is relevant in two dimensions for a general tensor coefficient **K**. It allows us to reduce the number of unknowns while keeping the accuracy of classical MHFEs. However, the system matrix is not always positive definite contrary to the standard MHFE method. Therefore, iterative solvers like conjugate gradients methods are no longer suited. The conditions to obtain a positive definite system depend on the shape of the triangular element and the tensor **K** (see equation (71)). This property of the final matrix is not required when direct solvers are used. In this case, a significant reduction of, say, 45%–50% CPU time can be obtained with the single-unknown formulation compared with the classical one [*Younes et al.*, 1999a]. Note that the single-unknown for-

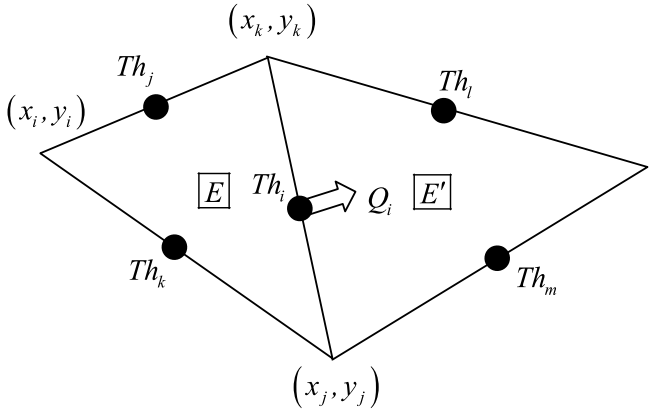

Figure 6. Numbering for the nonconforming finite element method.

mulation presented above cannot be extended to 3-D problems with general tetrahedral meshes, except for a very specific tetrahedral discretization [*Younes et al.*, 2004].

4. LINKS BETWEEN MIXED FINITE ELEMENTS AND OTHER METHODS

[58] The MFE method can be shown equivalent to other locally conservative discretization methods which handle discontinuous coefficients [*Brezzi et al.*, 2004; *Klausen and Russell*, 2005]. In sections 4.1–4.3 the relationships of the MFE method with the nonconforming finite element method, finite differences, and multipoint flux approximation methods are detailed.

4.1. MHFE and Nonconforming Finite Element Methods on Triangles

[59] The equivalence between RT0 on triangles and the nonconforming Crouzeix-Raviart [*Crouzeix and Raviart*, 1973] finite elements was shown more than 20 years ago [*Marini*, 1985]. The nonconforming finite element method uses the chapeau functions as basis functions like the standard finite element method. However, seed nodes are the midpoints of the edges; that is, $\phi_{E,i}(x, y) = 1$ at the midpoint of the edge i of coordinates $((x_j + x_k)/2, (y_j + y_k)/2)$ and zero at the midpoints of edges j and k (see Figure 6).

[60] As for the standard finite element method, the pressure head h is considered to be piecewise linear:

$$h = \sum_{i=1}^{\mathrm{Ned}} Th_i\, \phi_i(x,y), \tag{73}$$

where Th_i is the local pressure head at edge i and $\phi_i(x, y)$ is the chapeau function defined as

$$\phi_i(x,y) = \begin{cases} \phi_{E,i}(x,y) & \text{on} \quad E \\ \phi_{E',i}(x,y) & \text{on} \quad E' \\ 0 & \text{elsewhere.} \end{cases} \tag{74}$$

Contrary to the mixed approach where the equations are discretized separately, Darcy's law is substituted in the mass balance equation yielding the diffusivity equation which is, in the elliptic (stationary) case, written as

$$\nabla \cdot (-\mathbf{K}\nabla h) = f. \tag{75}$$

The variational formulation is written by using $\phi_i(x, y)$ as test functions:

$$\int_\Omega \nabla \cdot (-\mathbf{K}\nabla h)\phi_i = \int_\Omega f\phi_i. \tag{76}$$

[61] Given the property (74) of the functions $\phi_i(x, y)$ and by using integration by parts, the diffusivity equation (76) for the node (or the edge) i shared by the two elements E and E' can be rewritten as

$$\sum_{j=1}^{3} Th_{E,j} \int_E \nabla\phi_{E,i}\mathbf{K}_E\nabla\phi_{E,j} + \sum_{j=1}^{3} Th_{E',j} \int_{E'} \nabla\phi_{E',i}\mathbf{K}_{E'}\nabla\phi_{E',j} = \int_E f\phi_{E,i} + \int_{E'} f\phi_{E,j}. \tag{77}$$

Since $\phi_{E,i}(x, y)$ is a linear function, $\nabla\phi_{E,i}$ is constant, which transforms (77) into

$$|E| \sum_{j=1}^{3} Th_{E,j}\left(\nabla\phi_{E,i}\mathbf{K}_E\nabla\phi_{E,j}\right) + |E'| \sum_{j=1}^{3} Th_{E',j}\left(\nabla\phi_{E',i}\mathbf{K}_{E'}\nabla\phi_{E',j}\right) = \frac{Q_{E,s}}{3} + \frac{Q_{E',s}}{3}. \tag{78}$$

The constant gradient $\nabla\phi_{E,i}$ can be expressed as

$$\nabla\phi_{E,i} = \frac{1}{|E|}\mathbf{x}_{kj}^{\perp}, \tag{79}$$

where $\mathbf{x}_{kj}^{\perp}$ is a vector obtained by a $\pi/2$ rotation of $\mathbf{x}_{kj}$. Therefore, with a full tensor $\mathbf{K}_E$ one gets

$$|E|\left(\nabla\phi_{E,i}\mathbf{K}_E\nabla\phi_{E,j}\right) = \frac{\det(\mathbf{K}_E)}{|E|}\mathbf{x}_{jk}^T\left(\mathbf{K}_E^{-1}\right)\mathbf{x}_{ki}. \tag{80}$$

Thus, equation (78) can be rewritten as

$$-\frac{\det(\mathbf{K}_E)}{|E|}\left\{\left(\mathbf{x}_{jk}^T\,\mathbf{K}_E^{-1}\,\mathbf{x}_{jk}\right)Th_{E,i} + \left(\mathbf{x}_{jk}^T\,\mathbf{K}_E^{-1}\,\mathbf{x}_{ki}\right)Th_{E,j} + \left(\mathbf{x}_{jk}^T\mathbf{K}_E^{-1}\mathbf{x}_{ij}\right)Th_{E,k}\right\} + \{\ldots\}_{E'} = \frac{Q_{E,s}}{3} + \frac{Q_{E',s}}{3}. \tag{81}$$

[62] This equation drawn from the nonconforming finite element method is similar to (62) expressing the continuity of RT0 fluxes between two adjacent elements. Therefore, the RT0 MFE method for the elliptic case over triangles, even with a full tensor coefficient and sink/source terms, is strictly equivalent to the nonconforming finite element method. This equivalence will be used later to develop a mass lumping scheme for the MHFE method.

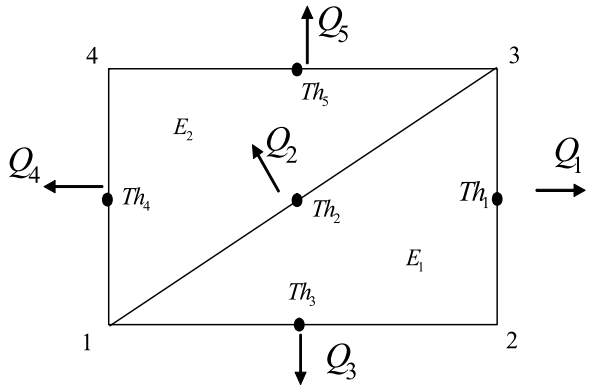

Figure 7. Calculation of fluxes for a rectangular element E subdivided into two triangles E_1 and E_2.

4.2. MHFE and the Finite Difference Method

[63] Here an equivalence is sought between the MHFE method reformulated with a new variable per element (see section 3.3) and the finite difference (FD) method without any quadrature formula. To this aim, consider a triangulation obtained by subdivision of rectangles with a diagonal tensor **K** constant per rectangle (Figure 7).

[64] The classical MHFE method on triangles is equivalent to the single-unknown formulation for which fluxes through edges of triangles are given by (64). Each triangle E_1 and E_2 encloses an angle of $\pi/2$. Therefore, by using (68) and the indexation of Figure 7, the following relationship can be obtained:

$$H_{E1} = H_{E2} = Th_2 = H_E, \tag{82}$$

where H_E is the head for the rectangle E. The fluxes obtained from (64) reduce to

$$\begin{aligned} Q_1 &= 2\frac{\Delta x}{\Delta y}\Big|_E \mathbf{K}_{E,x}(H_E - Th_1), \\ Q_4 &= 2\frac{\Delta x}{\Delta y}\Big|_E \mathbf{K}_{E,x}(H_E - Th_4), \\ Q_3 &= 2\frac{\Delta y}{\Delta x}\Big|_E \mathbf{K}_{E,y}(H_E - Th_3), \\ Q_5 &= 2\frac{\Delta y}{\Delta x}\Big|_E \mathbf{K}_{E,y}(H_E - Th_5), \end{aligned} \tag{83}$$

where Δx and Δy are the length and width of the rectangular element E.

[65] By using the continuity of the fluxes and heads at edges between adjacent rectangles, each flux in (83) across an edge can be expressed as a function of the mean heads at the two rectangles sharing that edge (similarly to (69)). Then, these expressions are substituted in the mass balance equation over the rectangle ($Q_1 + Q_3 + Q_4 + Q_5 = 0$) which leads to the standard FD scheme on rectangles with a five-point stencil. Therefore, the MHFE method on triangles formed by the subdivision of rectangles is algebraically equivalent to the FD method on the parent rectangular grid. It remains that MHFE is less efficient since it uses 3 times more unknowns than the finite difference method. Note that for a 2-D problem with full tensor coefficients, this equivalence does not hold (in this case $H_{E1} \neq H_{E2} \neq H_E$).

4.3. MHFE and the Multipoint Flux Approximation Method

[66] The multipoint flux approximation (MPFA) method is a control volume formulation, where more than two pressure values are used in the flux approximation [*Aavatsmark et al.*, 1998a, 1998b]. The first derivation of the method was published in 1994 [*Aavatsmark et al.*, 1994; *Edwards and Rogers*, 1994]. In contrast to MFEs, the MPFA method gives fluxes at cell interfaces explicitly by weighted sums of discrete node pressures. The MPFA method can be applied in the physical space or in the reference space. Reference space discretizations are symmetric, but their convergence diminishes or vanishes for rough quadrangular grids [*Aavatsmark et al.*, 2007]. On the other hand, physical space approximations have good convergence properties but are nonsymmetric for quadrilaterals which are not parallelograms [*Aavatsmark et al.*, 2007].

[67] When numerical approximations or quadrature rules are used, relationships can be found between MPFA variants and MFEs. For instance, the reference space MPFA method was shown equivalent to MFEs by *Klausen and Winther* [2006a] and *Wheeler and Yotov* [2006a, 2006b]. In the work by *Klausen and Winther* [2006b], a MFE method with broken Raviart-Thomas elements and nonconventional quadrature rule was shown equivalent to the MPFA derived in the physical space. For triangular meshes, *Vohralik* [2006] proved that the RT0 MFE method was similar to a particular nonsymmetric MPFA method, and this was done without any numerical integration. In sections 4.3.1–4.3.4, the links between MPFA and MHFE formulations of both RT0 and BDM1 methods on triangular meshes are established algebraically.

4.3.1. Multipoint Flux Approximation Method on Triangles

[68] The basic idea prevailing in MPFA is to divide each triangle into three subcells (see Figure 8 for the splitting into subcells and notations). Inside, e.g., the subcell ($\mathbf{x}_i$, $\mathbf{x}_i^2$, $\overline{\mathbf{x}}$, $\mathbf{x}_i^1$), a linear variation of the pressure head is postulated and

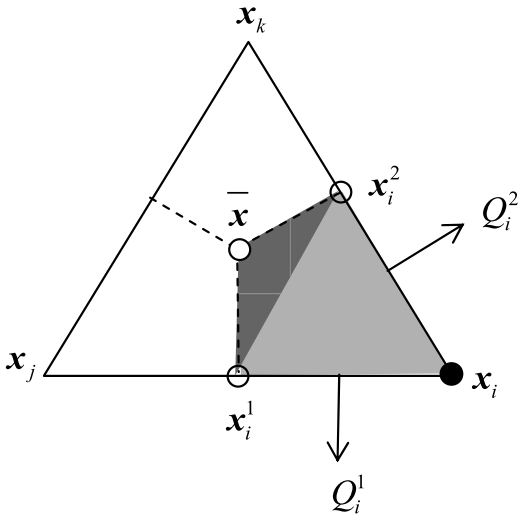

Figure 8. Triangle splitting into three subcells and linear head approximation on each subcell.

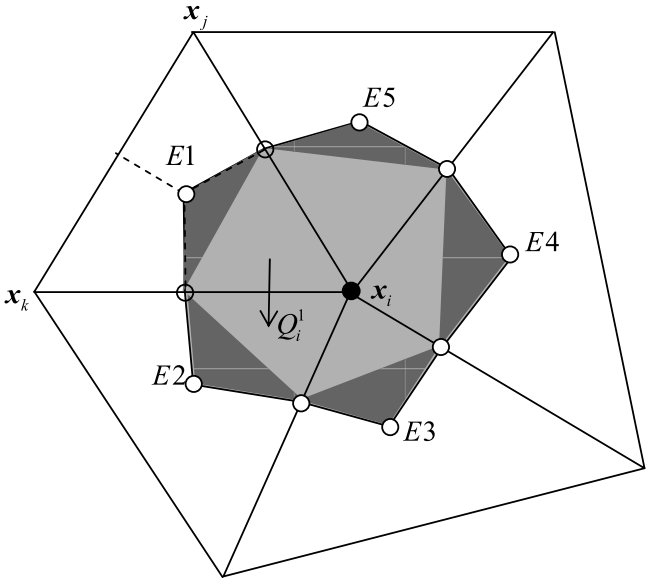

Figure 9. The interaction region sharing the vertex *i*.

defined by the pressure heads λ_i^1 at the midpoint edge $\mathbf{x}_i^1$, λ_i^2 at the midpoint edge $\mathbf{x}_i^2$, and h_E at the center $\bar{x}$ of element E (Figure 8).

[69] With these settings, the fluxes at subedges (half edges) $Q_i^1 = \int_{x_i}^{x_i^1} -\mathbf{K}_E \nabla h \cdot \mathbf{n}_1$ and $Q_i^2 = \int_{x_i}^{x_i^2} -\mathbf{K}_E \nabla h \cdot \mathbf{n}_2$, taken positive for outflow, are given by

$$\begin{pmatrix} Q_i^1 \\ \\ Q_i^2 \end{pmatrix} = \underbrace{\frac{1}{2\left|S_{\bar{\mathbf{x}}\mathbf{x}_i^1\mathbf{x}_i^2}\right|} \begin{pmatrix} \left(\mathbf{x}_i^1 - \mathbf{x}_i\right)^{\perp} \mathbf{K}_E \left(\mathbf{x}_i^2 - \bar{\mathbf{x}}\right)^{\perp} & \left(\mathbf{x}_i^1 - \mathbf{x}_i\right)^{\perp} \mathbf{K}_E \left(\bar{\mathbf{x}} - \mathbf{x}_i^1\right)^{\perp} \\ \\ \left(\mathbf{x}_i - \mathbf{x}_i^2\right)^{\perp} \mathbf{K}_E \left(\mathbf{x}_i^2 - \bar{\mathbf{x}}\right)^{\perp} & \left(\mathbf{x}_i - \mathbf{x}_i^2\right)^{\perp} \mathbf{K}_E \left(\bar{\mathbf{x}} - \mathbf{x}_i^1\right)^{\perp} \end{pmatrix}}_{\mathbf{G}_{E,i}} \cdot \begin{pmatrix} \lambda_i^1 - h_E \\ \\ \lambda_i^2 - h_E \end{pmatrix}, \tag{84}$$

where $|S_{\bar{\mathbf{x}}\mathbf{x}_i^1\mathbf{x}_i^2}|$ is the surface area of the triangle spanning between the points $\bar{\mathbf{x}}$, $\mathbf{x}_i^1$, and $\mathbf{x}_i^2$ and, e.g., $(\mathbf{x}_i^1 - \mathbf{x}_i)^{\perp}$ is a $\pi/2$ rotation of the vector $\mathbf{x}_i^1 - \mathbf{x}_i$. All subcells sharing the vertex $\mathbf{x}_i$ create an interaction region (Figure 9).

[70] The discretization of the flow equation is performed by assuming continuity of both fluxes and pressure heads for each subedge. With these assumptions, an explicit discrete expression of fluxes can be found after solving a local linear system and after algebraic elimination of heads λ_i^j at each subedge within the interaction volume (see *Aavatsmark* [2002] for details). For each subedge, the flux can then be written explicitly as a weighted sum of the cell heads within the interaction volume. In the example sketched in Figure 9, the flux Q_i^1, for example, is written as

$$Q_i^1 = \sum_{k=1}^{5} t_i^k h_{Ek}, \tag{85}$$

where t_i^k are transmissibility coefficients and h_{Ek} are mean heads located at the gravity center of triangles of the original mesh. The final MPFA system is obtained by writing a mass balance equation over each triangle; that is, the sum of the six subedge fluxes of the element equals the sink/source terms over that element. However, the resulting matrix of the complete system is nonsymmetric since the local matrix $\mathbf{G}_{E,i}$ in (84) is nonsymmetric too.

[71] As shown by *Pal et al.* [2006], there exists some flexibility in the location of each continuity point along the edges of the triangle. A continuity point can be located between the edge midpoint and the vertex *i* (Figure 8). The symmetry is achieved when the continuity point is located at $w = 2/3$ ($w = |\mathbf{x}_i^1 - \mathbf{x}_i|/|\overline{\mathbf{x}_{ij}} - \mathbf{x}_i|$ where $\overline{\mathbf{x}_{ij}} = (\mathbf{x}_i + \mathbf{x}_j)/2$). In this case, $\mathbf{x}_i^1$, $\mathbf{x}_i$, $\mathbf{x}_i^2$, and $\bar{\mathbf{x}}$ is a parallelogram, and the local matrix $\mathbf{G}_{E,i}$ of expression (84) can be replaced by the following symmetric matrix:

$$\mathbf{G}_{E,i}^{\mathrm{sym}} = \frac{1}{2\left|S_{\bar{\mathbf{x}}\mathbf{x}_i^1\mathbf{x}_i^2}\right|} \cdot \begin{pmatrix} \left(\overline{\mathbf{x}_{ij}} - \mathbf{x}_i\right)^{\perp} \mathbf{K}_E \left(\mathbf{x}_i^2 - \bar{\mathbf{x}}\right)^{\perp} & \left(\overline{\mathbf{x}_{ij}} - \mathbf{x}_i\right)^{\perp} \mathbf{K}_E \left(\bar{\mathbf{x}} - \mathbf{x}_i^1\right)^{\perp} \\ \left(\mathbf{x}_i - \overline{\mathbf{x}_{ik}}\right)^{\perp} \mathbf{K}_E \left(\mathbf{x}_i^2 - \bar{\mathbf{x}}\right)^{\perp} & \left(\mathbf{x}_i - \overline{\mathbf{x}_{ik}}\right)^{\perp} \mathbf{K}_E \left(\bar{\mathbf{x}} - \mathbf{x}_i^1\right)^{\perp} \end{pmatrix}. \tag{86}$$

4.3.2. MPFA Formulation of RT0

[72] This part derives the algebraic link between triangular RT0 MHFE and MPFA formulations as developed by *Vohralik* [2004, 2006]. Recall that with MHFEs on triangles, the steady state mass conservation equation given in (32) is written as $\sum_{i=1}^{3} Q_{\partial E,i} = Q_{E,s}$, and the discretization of Darcy's law given in (31) is

$$Q_{\partial E,i} = \sum_{k=1}^{3} B_{E,i,k}^{-1} \left(h_E - Th_{\partial E,k}\right). \tag{87}$$

[73] The inverse of the matrix $\mathbf{B}_E$ for triangles is given by (61). Equation (87) is substituted in the mass balance equation, and the value of $Th_{\partial E,1}$ is expressed from this equation as a function of $Th_{\partial E,2}$, $Th_{\partial E,3}$, and $Q_{E,s}$. Then, $Th_{\partial E,1}$ is reintroduced into expression (87) to calculate $Q_{\partial E,1}$ and $Q_{\partial E,2}$. This yields

$$\begin{pmatrix} Q_{\partial E,3} \\ \\ Q_{\partial E,2} \end{pmatrix} = \frac{\det(\mathbf{K}_E)}{|E|} \begin{pmatrix} \mathbf{x}_{12}\mathbf{K}_E^{-1}(\mathbf{x}_{23} - \mathbf{x}_{12}) & \mathbf{x}_{12}\mathbf{K}_E^{-1}(\mathbf{x}_{23} - \mathbf{x}_{31}) \\ \\ \mathbf{x}_{31}\mathbf{K}_E^{-1}(\mathbf{x}_{23} - \mathbf{x}_{12}) & \mathbf{x}_{31}\mathbf{K}_E^{-1}(\mathbf{x}_{23} - \mathbf{x}_{31}) \end{pmatrix} \cdot \begin{pmatrix} Th_{\partial E,3} - h_E \\ \\ Th_{\partial E,2} - h_E \end{pmatrix} + Q_{E,s} \begin{pmatrix} \frac{\det(\mathbf{K}_E)}{|E|}\left(\mathbf{x}_{12}\mathbf{K}_E^{-1}\mathbf{x}_{23}\right)L_E + \frac{1}{3} \\ \\ \frac{\det(\mathbf{K}_E)}{|E|}\left(\mathbf{x}_{32}\mathbf{K}_E^{-1}\mathbf{x}_{23}\right)L_E + \frac{1}{3} \end{pmatrix}. \tag{88}$$

Using the following properties on triangles,

$$\frac{\det(\mathbf{K}_E)}{|E|}\mathbf{x}_{ij}\mathbf{K}_E^{-1}(\mathbf{x}_{jk}-\mathbf{x}_{ij}) = \frac{1}{4\left|S_{\overline{x}x_i^1x_i^2}\right|}(\mathbf{x}_i^1-\mathbf{x}_i)^{\perp}\mathbf{K}_E(\mathbf{x}_i^2-\overline{\mathbf{x}})^{\perp},$$
$$\frac{\det(\mathbf{K}_E)}{|E|}\mathbf{x}_{ij}\mathbf{K}_E^{-1}(\mathbf{x}_{jk}-\mathbf{x}_{ki}) = \frac{1}{4\left|S_{\overline{x}x_i^1x_i^2}\right|}(\mathbf{x}_i^1-\mathbf{x}_i)^{\perp}\mathbf{K}_E(\overline{\mathbf{x}}-\mathbf{x}_i^1)^{\perp}, \tag{89}$$

the two fluxes in (88) become

$$\begin{pmatrix} Q_{\partial E,3} \\ \\ Q_{\partial E,2} \end{pmatrix} = \frac{1}{4\left|S_{\overline{x}x_1^1x_1^2}\right|} \cdot \begin{pmatrix} (\mathbf{x}_1^1-\mathbf{x}_1)^{\perp}\mathbf{K}_E(\mathbf{x}_1^2-\overline{\mathbf{x}})^{\perp} & (\mathbf{x}_1^1-\mathbf{x}_1)^{\perp}\mathbf{K}_E(\overline{\mathbf{x}}-\mathbf{x}_1^1)^{\perp} \\ \\ (\mathbf{x}_1-\mathbf{x}_1^2)^{\perp}\mathbf{K}_E(\mathbf{x}_1^2-\overline{\mathbf{x}})^{\perp} & (\mathbf{x}_1-\mathbf{x}_1^2)^{\perp}\mathbf{K}_E(\overline{\mathbf{x}}-\mathbf{x}_1^1)^{\perp} \end{pmatrix} \cdot \begin{pmatrix} Th_{\partial E,3}-h_E \\ \\ Th_{\partial E,2}-h_E \end{pmatrix} + Q_{E,s}\begin{pmatrix} \frac{\det(\mathbf{K}_E)}{|E|}(\mathbf{x}_{12}\mathbf{K}_E^{-1}\mathbf{x}_{23})L_E+\frac{1}{3} \\ \\ \frac{\det(\mathbf{K}_E)}{|E|}(\mathbf{x}_{32}\mathbf{K}_E^{-1}\mathbf{x}_{23})L_E+\frac{1}{3} \end{pmatrix}. \tag{90}$$

Therefore, the half-edge fluxes with hybrid RT0 can be written in the following form:

$$\begin{pmatrix} Q_{\partial E,3}/2 \\ \\ Q_{\partial E,2}/2 \end{pmatrix} = [\mathbf{G}_{E,1}]\begin{pmatrix} Th_{\partial E,3}-h_E \\ \\ Th_{\partial E,2}-h_E \end{pmatrix} + Q_{E,s}\begin{pmatrix} \frac{\det(\mathbf{K}_E)}{2|E|}(\mathbf{x}_{12}\mathbf{K}_E^{-1}\mathbf{x}_{23})L_E+\frac{1}{6} \\ \\ \frac{\det(\mathbf{K}_E)}{2|E|}(\mathbf{x}_{32}\mathbf{K}_E^{-1}\mathbf{x}_{23})L_E+\frac{1}{6} \end{pmatrix}, \tag{91}$$

where $[\mathbf{G}_{E,1}]$ is the matrix defined by equation (84). This form in (90), directly stemming from MHFEs, looks similar to the general formulation of the MPFA approach. Identification between (91) and (84) simply yields $Q_i^1 = Q_{\partial E,3}/2$, $Q_i^2 = Q_{\partial E,2}/2$, $\lambda_i^1 = Th_{\partial E,3}$, and $\lambda_i^2 = Th_{\partial E,2}$.

[74] In the case of steady state flow without sink/source terms, (91) reduces to (84), and the hybrid mixed formulation of RT0 rewritten in MPFA formalism is algebraically equivalent to the standard MPFA method. It must be mentioned that sink/source terms are not treated in the same way. For the MHFE-based formulation, each subedge flux is written explicitly as a weighted sum of not only the cell pressure heads but also the cell sink/source terms of the elements in the interaction volume [*Vohralik*, 2006].

4.3.3. MPFA Formulation of BDM1

[75] Again, MHFE equations are manipulated to derive a form similar to the MPFA system (84). In the case of BDM1 and contrary to RT0, numerical integration is required at the scale of each element. The local matrix $\mathbf{B}_E$ of BDM1 given in (41) is evaluated by using a quadrature rule [*Wheeler and Yotov*, 2006b]. The integrals are transferred to the reference space (see Appendix A) and evaluated with the point values at the vertices of the reference triangle (with coordinates (0, 0), (1, 0), (0,1)):

$$B_{E,i,j,k,l} = \int_{\widehat{E}} \widehat{\omega}_{E,i,j}^{\mathrm{BDM1,T}}\widehat{\mathbf{K}}^{-1}\widehat{\omega}_{E,k,l}^{\mathrm{BDM1}} \simeq \frac{|\widehat{E}|}{3}\left[\left(\widehat{\omega}_{E,i,j}^{\mathrm{BDM1,T}}\widehat{\mathbf{K}}^{-1}\widehat{\omega}_{E,k,l}^{\mathrm{BDM1}}\right)_{(0,0)} + \left(\widehat{\omega}_{E,i,j}^{\mathrm{BDM1,T}}\widehat{\mathbf{K}}^{-1}\widehat{\omega}_{E,k,l}^{\mathrm{BDM1}}\right)_{(1,0)} + \left(\widehat{\omega}_{E,i,j}^{\mathrm{BDM1,T}}\widehat{\mathbf{K}}^{-1}\widehat{\omega}_{E,k,l}^{\mathrm{BDM1}}\right)_{(0,1)}\right]. \tag{92}$$

[76] Recall that the BDM1 vector basis functions are set up to verify (26), namely, for an edge l formed by the two end points r_{lk} (k = 1,2) with a normal vector $\mathbf{n}_{\partial E_l}$:

$$\widehat{\omega}_{E,i,j}^{\mathrm{BDM1}}(r_{lk})n_{\partial E_l} = \frac{2}{|E_l|}\delta_{il}\delta_{jk} \text{ for } l = 1,..,3 \text{ and } k = 1,2. \tag{93}$$

Therefore, handling (92) and (93) to compute the local matrix $\mathbf{B}_E$ results in a block-diagonal matrix where only the two vector basis functions associated with a corner (x_i, y_i) are coupled. The (6 × 6) linear system (40) reduces to three (2 × 2) linear systems (one for each vertex). Taking, for example, the vertex 1 of coordinates (0,0), only $\widehat{\omega}_{E,3,1}^{\mathrm{BDM1}}$ and $\widehat{\omega}_{E,2,2}^{\mathrm{BDM1}}$ are nonzero (see Figure 3), and the corresponding (2 × 2) local system is

$$\frac{1}{6}\begin{pmatrix} \left(\widehat{\omega}_{E,3,1}^{\mathrm{BDM1,T}}\widehat{\mathbf{K}}_E^{-1}\widehat{\omega}_{E,3,1}^{\mathrm{BDM1,T}}\right)_{(0,0)} & \left(\widehat{\omega}_{E,3,1}^{\mathrm{BDM1,T}}\widehat{\mathbf{K}}_E^{-1}\widehat{\omega}_{E,2,2}^{\mathrm{BDM1}}\right)_{(0,0)} \\ \left(\widehat{\omega}_{E,3,1}^{\mathrm{BDM1,T}}\widehat{\mathbf{K}}_E^{-1}\widehat{\omega}_{E,2,2}^{\mathrm{BDM1}}\right)_{(0,0)} & \left(\widehat{\omega}_{E,2,2}^{\mathrm{BDM1,T}}\widehat{\mathbf{K}}_E^{-1}\widehat{\omega}_{E,2,2}^{\mathrm{BDM1}}\right)_{(0,0)} \end{pmatrix} \cdot \begin{pmatrix} Q_{\partial E,3,1} \\ \\ Q_{\partial E,2,2} \end{pmatrix} = \begin{pmatrix} h_E - Th_{\partial E,3,1} \\ \\ h_E - Th_{\partial E,2,2} \end{pmatrix}. \tag{94}$$

[77] Substituting expressions from Appendix B of $\widehat{\omega}_{E,3,1}^{\mathrm{BDM1},T}$ and $\widehat{\omega}_{E,2,2}^{\mathrm{BDM1}}$ in (94) and inverting the resulting system yields the following formulation:

$$\begin{pmatrix} Q_{\partial E,3,1} \\ \\ Q_{\partial E,2,2} \end{pmatrix} = \left[\mathbf{G}_{E,i}^{\mathrm{sym}}\right]\begin{pmatrix} Th_{\partial E,3,1}-h_E \\ \\ Th_{\partial E,2,2}-h_E \end{pmatrix}, \tag{95}$$

where $[\mathbf{G}_{E,i}^{\mathrm{sym}}]$ is the local matrix given in (86). By identifying the rearranged BDM1-MHFE system in (95) and the MPFA symmetric system in (84), it is obvious that both methods are equivalent: $Q_i^1 = Q_{\partial E,3,1}$, $Q_i^2 = Q_{\partial E,2,2}$, $\lambda_i^1 = Th_{\partial E,3,1}$, and $\lambda_i^2 = Th_{\partial E,2,2}$.

4.3.4. Comparison of Hybrid and MPFA Formulations of RT0 and BDM1

[78] In this section, four mixed formulations for triangles are compared: (1) the hybrid form of RT0 (one pressure head per edge for the unknowns), (2) the hybrid form of BDM1 (two pressure heads per edge for the unknowns), (3) the MPFA form of RT0 (one pressure head per element for the unknowns), and (4) the MPFA form of BDM1 (one pressure head per element for the unknowns). Main properties of these four mixed formulations are summarized in Table 1.

TABLE 1. Properties of Hybrid-RT0, MPFA-RT0, Hybrid-BDM1, and MPFA-BDM1 Formulations

	Hybrid-RT0	MPFA-RT0	Hybrid-BDM1	MPFA-BDM1
Numerical quadrature	no	no	no	yes
Symmetric and positive definite matrix	yes	no	yes	yes
Number of unknowns	number of edges	number of elements	2 × number of edges	number of elements
Stencil	5	≈15	10	≈15

[79] The comparisons carried out by *Younes and Fontaine* [2008b] for heterogeneous domains and unstructured triangular meshes result in the following main conclusions: (1) the MPFA-RT0 is the less efficient method because of the nonsymmetric character of the linear system to solve which can be indefinite [*Vohralik*, 2006]; (2) the Hybrid-BDM1 formulation requires less CPU time than Hybrid-RT0 to achieve the same accuracy of the velocity field; (3) for the same computation effort, MPFA-BDM1 is more accurate than Hybrid-RT0 but less accurate than Hybrid-BDM1; and (4) in general, the accuracy of MPFA-BDM1 does not deteriorate with highly unstructured triangular meshes (contrary to quadrilateral meshes for which a lack of convergence can be encountered with rough grids).

[80] These results are in agreement with previous works by *Bergamaschi et al.* [1994], *Matringe et al.* [2006], and *Bause* [2008]. The point is that BDM1 formulations (Hybrid-BDM1 and MPFA-BDM1) often require less CPU time than Hybrid-RT0 to provide accurate velocity fields.

5. MONOTONICITY AND STABILITY OF THE MFE METHOD

[81] The MHFE method yields a symmetric and positive definite matrix which generally does not satisfy the *M* matrix property [*Hoteit et al.*, 2002a, 2002b; *Mazzia*, 2008; *Younes and Fontaine*, 2008a]. The obtained MFE solution may contain unphysical oscillations. In this section, the behavior of MFE solutions is studied for steady state problems when the diffusion tensor is heterogeneous and anisotropic and for transient problems.

5.1. Monotonicity of the MFE Method for Steady State Problems

[82] MFE like finite elements and finite volumes fail to preserve positivity of a continuum solution when the diffusion tensor is heterogeneous and anisotropic or the computational mesh is strongly perturbed. To preserve the positivity of the solution, the method must satisfy the so-called discrete maximum principle; that is, local maxima or minima do not appear in the numerical solution for a domain free of local sink/source terms. Therefore, the resulting numerical state variable and its related fluxes are consistent with the continuity of the physics supposedly mimicked by the discrete equations. A way to guarantee the respect of the discrete maximum principle is to obtain a final matrix which satisfies the *M* matrix property (i.e., nonsingular matrix with $m_{ii} > 0$ and $m_{ij} \leq 0$). Note that the *M* matrix property is sufficient but not necessary to respect the discrete maximum principle. The property *M* is difficult to satisfy with MHFE matrices. This can be shown easily with the case of scalar conductivity and rectangular shaped element $\Delta x \times \Delta y$.

5.1.1. MHFE Method on Rectangles

[83] The system matrix of the MHFE method is obtained by writing the continuity of fluxes between two adjacent elements *A* and *B*. From (34) and (35), the diagonal and off-diagonal terms of the final matrix can be written as

$$\begin{aligned} m_{ii} &= \left[B_{ii}^{-1} - \frac{\alpha_i^2}{\alpha}\right]_A + \left[B_{ii}^{-1} - \frac{\alpha_i^2}{\alpha}\right]_B . \\ m_{ij} &= \left[B_{ij}^{-1} - \frac{\alpha_i \alpha_j}{\alpha}\right]_A \end{aligned} \tag{96}$$

The elemental matrix $\mathbf{B}^{-1}$ for a rectangular element *A* is

$$\mathbf{B}_A^{-1} = 2\begin{pmatrix} 2\delta_x^A & \delta_x^A & 0 & 0 \\ \delta_x^A & 2\delta_{bfx}^A & 0 & 0 \\ 0 & 0 & 2\delta_y^A & \delta_y^A \\ 0 & 0 & \delta_y^A & 2\delta_y^A \end{pmatrix}, \tag{97}$$

where $\delta_x^A = \frac{\Delta y}{\Delta x} K^A$, $\delta_y^A = \frac{\Delta x}{\Delta y} K^A$, $\alpha_1 = \alpha_2 = 6\delta_x^A$, $\alpha_3 = \alpha_4 = 6\delta_y^A$, and $\alpha = 12(\delta_x^A + \delta_y^A)$. In view of (96) and (97), the diagonal terms m_{ii} are always positive since

$$B_{ii}^{-1} > \alpha_i^2/\alpha \text{ for } i = 1, 2, 3, 4. \tag{98}$$

On the other hand, getting negative off-diagonal terms yields the following conditions, e.g.,

$$m_{12} = B_{12}^{-1} - \frac{\alpha_1 \alpha_2}{\alpha} = \frac{\delta_x^A \delta_y^A}{\delta_x^A + \delta_y^A}\left(2 - \delta_x^A \Big/ \delta_y^A\right) \leq 0 \text{ if } \delta_x^A \Big/ \delta_y^A \geq 2 \tag{99}$$

$$m_{34} = B_{34}^{-1} - \frac{\alpha_3 \alpha_4}{\alpha} = \frac{\delta_y^A \delta_x^A}{\left(\delta_x^A + \delta_y^A\right)}\left(2 - \delta_y^A \Big/ \delta_x^A\right) \leq 0 \quad \text{if } \delta_x^A \Big/ \delta_y^A \leq 1/2. \tag{100}$$

[84] Obviously, conditions (99) and (100) cannot be fulfilled at the same time, and therefore, the matrix system of MHFE is never an *M* matrix in this case. The same study for triangular elements shows that the MHFE matrix is an *M* matrix in the case of a weakly acute triangulation (all angles are $<\pi/2$) [*Brezzi and Fortin*, 1991].

5.1.2. Improving the Monotonicity of the MHFE Method

[85] In the case of rectangles and diagonal conductivity tensor, a way to improve monotonicity of MHFEs is to use the quadrature formula (43) leading to a diagonal local matrix **B**. The MHFE method reduces to a five-point cell-centered FD scheme with a harmonic mean of conductivity at interfaces between cells. It is easy to show that the corresponding matrix is an *M* matrix.

[86] In the case of nonrectangular parallelograms with diagonal **K** or in the case of rectangular elements and full tensor coefficients, the same quadrature rule (43) allows transformation of the BDM1-MHFE method into a MPFA method. The resulting scheme is a nine-point cell-centered FD scheme with a generalized form of harmonic mean of conductivity at interfaces between cells [*Aavatsmark et al.*, 2007]. However, the resulting matrix is not an *M* matrix in general [*Edwards and Rogers*, 1998] even though this MPFA formulation of MHFEs improves the monotonicity and reduces the occurrence of unphysical oscillations [*Younes and Fontaine*, 2008a].

[87] Note that *Mlacnik and Durlofsky* [2006] developed a method for optimizing unstructured grids to improve the monotonicity of the MPFA method. *Nordbotten and Eigestad* [2005] and *Chen et al.* [2008] also developed new MPFA formulations improving monotonicity for strongly anisotropic domains.

[88] Another approach to reinforce the capability of MFEs to obey the discrete maximum principle was recently proposed by *Nakshatrala and Valocchi* [2009]. The basic idea of the method is to rewrite the MFE formulation as a problem of optimization under linear constraints explicitly introduced to satisfy positivity of the solution. This technique may, however, induce violation of the local mass balance in a part of the domain [*Nakshatrala and Valocchi*, 2009].

5.2. Improving the Stability of Triangular MHFE for Transient Problems

[89] For steady state problems handled with triangular MHFEs, the resulting matrix is an *M* matrix in the case of a weakly acute triangulation (all angles are $<\pi/2$) [*Brezzi and Fortin*, 1991]. This condition on angles is no longer sufficient for parabolic (transient) problems. A first approach to preserve the *M* matrix property is to change the Raviart-Thomas finite element space for the flux variable [*Marini and Pietra*, 1990]. Another technique commonly used in finite element methods is the so-called mass lumping. Basically, mass lumping consists of making diagonal (or "as diagonal as possible") the elemental matrix attached to the accumulation term in $\partial/\partial t$.

[90] A recent mass lumping procedure, suitable for various shapes of 2-D elements, was developed by *Younes et al.* [2006] without resorting to any numerical integration. The basic idea of this procedure is (1) to calculate steady state fluxes by using the classical MHFE method and (2) to add the accumulation and sink/source terms directly on the edges. In this procedure, the MHFE method is seen as a nonconforming finite element method. This scheme was shown to be efficient by smoothing unphysical oscillations for transient saturated flow problems [*Younes et al.*, 2006].

[91] In the following, it is shown how the mass lumping procedure can be set up for MHFE over triangles. The benefit of this technique is illustrated by mimicking transient two-phase flow (air plus water) in a porous medium initially dry and subjected to infiltration of water. Even though the physical relevance of mimicking infiltration by using Richards's equation can be deeply questioned, the equation remains largely used for unsaturated flow. Here this equation is just used for the purpose of illustration, knowing that the nonlinearity of the problem emphasizes discrepancies due to violations of the discrete maximum principle.

[92] The flux $Q_{\partial E,i}$ in transient conditions with an implicit scheme of RT0-MHFEs is given by (34) and recalled here:

$$Q_{\partial E,i}^{n+1} = \sum_{j=1}^{\mathrm{Ned}_E} N_{E,ij} Th_{\partial E,j}^{n+1} + F_{E,i}^{n}, \tag{101}$$

where

$$N_{E,ij} = \frac{\alpha_{E,i}\alpha_{E,j}}{\beta_E} - B_{E,ij}^{-1}, \tag{102}$$

$$F_{E,i}^{n} = \lambda_E \frac{\alpha_{E,i}}{\beta_E} h_E^n + \frac{\alpha_{E,i}}{\beta_E} Q_{E,s},$$

$$\lambda_E = \frac{c_E|E|}{\Delta t},$$

$$\alpha_{E,i} = \sum_{j=1}^{\mathrm{Ned}_E} B_{E,ij}^{-1},$$

$$\alpha_E = \sum_{i=1}^{\mathrm{Ned}_E} \alpha_{E,i},$$

$$\beta_E = (\lambda_E + \alpha_E).$$

With the hybrid formulation, each row i of the global system represents the continuity of fluxes between two adjacent elements E and E' sharing the edge i (the sum of the two fluxes $Q_{\partial E,i}$ and $Q_{\partial E',i}$ is null). Therefore, in view of (101), the global matrix will be an *M* matrix provided all local matrices $\mathbf{N}_E$ and $\mathbf{N}_{E'}$ are of type *M*.

[93] For triangles and scalar conductivity, the local matrix $\mathbf{N}_E$ simplifies (using (61)) into

$$\mathbf{N}_E = -K_E \begin{bmatrix} \frac{\mathbf{x}_{23}^2}{|E|} & -2\cot(\varphi_{E,12}) & -2\cot(\varphi_{E,13}) \\ -2\cot(\varphi_{E,12}) & \frac{\mathbf{x}_{31}^2}{|E|} & -2\cot(\varphi_{E,23}) \\ -2\cot(\varphi_{E,13}) & -2\cot(\varphi_{E,23}) & \frac{\mathbf{x}_{12}^2}{|E|} \end{bmatrix} - \frac{\lambda_E}{3(3+\lambda_E L_E)} \begin{bmatrix} 1 & 1 & 1 \\ 1 & 1 & 1 \\ 1 & 1 & 1 \end{bmatrix}, \tag{103}$$

where $\varphi_{E,ij}$ is the angle between edges i and j, $\mathbf{x}_{ij}$ is the edge vector from node i toward node j, and L_E is the shape coefficient in (59). The diagonal terms of $\mathbf{N}_E$ are always positive whatever the parameters and the shape of the element. The off-diagonal terms are conditionally negative. For the elliptic case ($\lambda_E = 0$, steady state case), these terms are negative in the case of acute triangulation (all angles $<\pi/2$). For the parabolic (transient) case, it can be shown that $\mathbf{N}_E$ is of type M if the time step verifies [*Younes et al.*, 2006]:

$$\frac{1}{18}\frac{c_E}{K_E}\frac{|E|[\tan(\varphi) - 6L_E]}{\Delta t} < 1, \tag{104}$$

where φ is one of the three angles of the triangle E. Condition (104) is always verified (whatever Δt) for $0 \le \varphi \le 40.89°$ [*Younes et al.*, 2006], which obviously cannot be fulfilled for all angles of a triangle. Thus, for a given spatial acute triangulation and a given set of parameters, the global system is an M matrix only if the time step is large enough to fulfill condition (104).

[94] With the lumped formulation of the MHFE proposed by *Younes et al.* [2006], the stationary and the accumulation parts of the flux are distinguished:

$$Q^{n+1}_{\partial E,i} = \overline{Q}_{\partial E,i} + \frac{Q_{E,s}}{3} - \frac{\lambda_E}{3}\left(Th^{n+1}_{\partial E,i} - Th^{n}_{\partial E,i}\right), \tag{105}$$

where $\overline{Q}_{\partial E,i}$ is the flux corresponding to the stationary problem without sink/source terms.The expression of the flux in (101) is then replaced by the following one:

$$Q^{n+1}_{\partial E,i} = \sum_{j=1}^{\mathrm{Ned}_E} N^{\mathrm{lump}}_{E,ij} Th^{n+1}_{\partial E,j} + F^{n}_{E,i}, \tag{106}$$

where $F^{n}_{E,i} = \frac{\alpha_{E,i}}{\alpha_E} Q_{E,S} + \frac{\lambda_E}{3} Th^{n}_{\partial E,i}$ and the local matrix $\mathbf{N}^{\mathrm{lump}}_E$ is given by

$$\mathbf{N}^{\mathrm{lump}}_E = -K_E \begin{bmatrix} \frac{\mathbf{x}^2_{23}}{|E|} & -2\cot(\varphi_{E,12}) & -2\cot(\varphi_{E,13}) \\ -2\cot(\varphi_{E,12}) & \frac{\mathbf{x}^2_{31}}{|E|} & -2\cot(\varphi_{E,23}) \\ -2\cot(\varphi_{E,13}) & -2\cot(\varphi_{E,23}) & \frac{\mathbf{x}^2_{12}}{|E|} \end{bmatrix} - \frac{\lambda_E}{3}\begin{bmatrix} 1 & 0 & 0 \\ 0 & 1 & 0 \\ 0 & 0 & 1 \end{bmatrix}. \tag{107}$$

[95] Contrary to the local matrix $\mathbf{N}_E$ of the classical MHFE scheme, the matrix $\mathbf{N}^{\mathrm{lump}}_E$ of the lumped form is always of type M for an acute triangulation, irrespective of the size of the time step. It remains that this lumped formulation cannot guarantee the M matrix property for any general triangulation. However, the lumping procedure can still be useful since it improves the monotonous character of the scheme.

5.3. Lumped Formulation of MHFE for Unsaturated Flow Problems

[96] The illustrative example given here is drawn from works by *Belfort et al.* [2009] and deals with unsaturated flow. Because of the nonlinearity of the problem, the calculations are strongly exposed to unphysical oscillations and convergence problems, especially in the case depicted below of infiltration with sharp wetting fronts in dry soils. The MHFE method was used for the discretization of the widely used Richards's equation, even though its physical relevance for simulating air-water flow in soils can be questioned [e.g., *Glass et al.*, 1989; *Selker et al.*, 1992].

[97] Simulations were performed with the general settings of infiltration of water in a soil initially dry. Infiltration is performed at constant rate for a period of 1 day over four types of meshes: a general quadrangular mesh, a general triangular mesh, a Delaunay triangulation, and an acute triangulation. Small time steps of 5 s or large time steps of 200 s are used, and all simulations are calculated with the classical (101) and the lumped (106) formulations of the MHFE method.

[98] Given the simulation settings, the expected numerical solutions should be bounded [*Belfort et al.*, 2009]. The values of the pressure head calculated at the edges of the elements should range between 25 cm (the top Dirichlet boundary condition) and −1000 cm (the bottom Dirichlet boundary condition). Because of the violation of the discrete maximum principle, the calculated solution may give values less than −1000 cm. To quantify how badly the solution breaks the maximum principle, results are summarized by providing $h_{\min}$, the minimal negative values of the solutions, and err_g, the relative size in % of the total surface area of the domain where the maximum principle is not matched up. Table 2 reports on these values for a prescribed simulation time of 1600 s.

[99] Strong unphysical oscillations appear with the classical MHFE method even with the large time step $\Delta t = 200$ s. The minimal value $h_{\min}$ reaches −1313.8 cm with quadrangles, and 9.3% of the domain is subjected to unphysical oscillations. The shorter the time step, the larger the unphysical oscillations, and sometimes the nonlinear problem may not converge. For instance, the classical MHFEs with a time step of 5 s do not converge whatever the type of mesh used.

[100] Compared with the classical approach, the mass lumping formulation reduces the unphysical oscillations for the quadrangular meshing. The minimal value reaches −1009 cm, and <2% of the domain is concerned with this problem. When dealing with triangular meshes (general or Delaunay triangulation) and large time steps of 200 s, the lumped formulation allows a significant reduction of the unphysical oscillations, and <0.1% of the domain is subjected to anomalies. As expected with acute triangulations, the lumped formulation results in a matrix of type M, and therefore, all unphysical discrepancies are eradicated. Contrary to the classical formulation, a decrease of the time step does not alter capabilities of the lumped formulation to solve

TABLE 2. Results of the Standard and Lumped Formulation for the Infiltration Problem at t = 1600 s[a]

	Quadrangles		General Triangles		Delaunay Triangles		Acute Triangles	
Δt (s)	err_g	h_{min}	err_g	h_{min}	err_g	h_{min}	err_g	h_{min}
				MHFE				
200	9.3%	−1313.8	2.9%	−1171.4	3%	−1186.4	5.7%	−1273.8
5	n.c.	n.c.	n.c.	n.c.	n.c.	n.c.	n.c.	n.c.
				Lumped MHFE				
200	1.3%	−1009	0.06%	−1000.04	0.02%	−1009.9	0.00%	−1000.00
5	1.1%	−1011.2	0.04%	−1000.03	1.49E-04	−1009.7	0.00%	−1000.00

[a]Abbreviation n.c. means convergence not reached.

correctly the nonlinear problem. In terms of unphysical oscillations, for a given spatial discretization, the results are almost similar to a 5 s or a 200 s time step.

5.4. A Technique for Improving the Stability of Quadrangular MHFE for Transient Problems

[101] As reported in Table 2, the unphysical oscillations with the lumped formulation remain much more important with quadrangles (err_g = 1.34%) than with triangles (err_g = 0.02%). It was shown by *Younes et al.* [2006] that the lumped formulation of MHFE never resulted in an M matrix with rectangular meshes, even for a homogeneous problem. However, the monotonicity of the lumped MHFE method on general quadrangular meshing can be improved by considering each quadrilateral as a macroelement of triangles. The idea of fictitious subdivision into triangles has already been discussed for mixed finite elements [*Brezzi and Fortin*, 1991; *Kuznetsov and Repin*, 2003; *Kuznetsov and Repin*, 2005; *Jaffré et al.*, 2006] and used in the mimetic finite element/finite difference methods [*Kuznetsov et al.*, 2004; *Lipnikov et al.*, 2006; *Brezzi et al.*, 2005a, 2005b].

[102] To make it simple, consider a quadrangular element E as the aggregation of two triangles A and B (Figure 10). Equation (106) for each triangle gives fluxes $Q_{\partial A,i}$ and $Q_{\partial B,i}$ as functions of the average pressure heads $Th_{\partial A,j}$ and $Th_{\partial B,j}$ on edges. The trick is to write the average pressure head of the interior edge as a function of the average heads at the four edges of the quadrangle. The continuity of fluxes and heads between triangles A and B (see Figure 10 for notations and numbering) results in the following expressions:

$$Q_{A,3}^{n+1} + Q_{B,3}^{n+1} = \sum_{j=1}^{3} N_{A,3j}^{\text{lump}}\, Th_{A,j}^{n+1} + F_{A,3}^{n} + \sum_{j=1}^{3} N_{B,3j}^{\text{lump}}\, Th_{B,j}^{n+1} + F_{B,3}^{n} = 0$$

$$Th_{\text{int}}^{n+1} = Th_{A,3}^{n+1} = Th_{B,3}^{n+1}, \tag{108}$$

which is transformed into

$$Th_{\text{int}}^{n+1} = \frac{-1}{N_{A,33}^{\text{lump}} + N_{B,33}^{\text{lump}}} \cdot \left(\sum_{j=1}^{2} N_{A,3j}^{\text{lump}}\, Th_{\partial A,j}^{n+1} + F_{A,3}^{n} + \sum_{j=1}^{2} N_{B,3j}^{\text{lump}}\, Th_{\partial B,j}^{n+1} + F_{B,3}^{n} \right). \tag{109}$$

[103] Inserting equation (109) in (106) (i.e., the lumped equations of fluxes for triangles), the fluxes of both triangles A and B are functions of heads at the exterior edges (i.e., the edges of the quadrangular element E). Therefore, it becomes possible to calculate the fluxes $Q_{\partial E,i}$ of a quadrangle by using equation (106) but with a modified matrix $\mathbf{N}$ and a modified vector F. For example, the flux across edge 1 of the quadrangular element E becomes

$$\begin{aligned} Q_{\partial E,1}^{n+1} = {} & \left[N_{B,11}^{\text{lump}} - \frac{N_{B,13}^{\text{lump}} N_{B,31}^{\text{lump}}}{N_{A,33}^{\text{lump}} + N_{B,33}^{\text{lump}}} \right] Th_{\partial E,1}^{n+1} \\ & + \left[\frac{-N_{A,31}^{\text{lump}} N_{B,13}^{\text{lump}}}{N_{A,33}^{\text{lump}} + N_{B,33}^{\text{lump}}} \right] Th_{\partial E,2}^{n+1} + \left[N_{B,12}^{\text{lump}} - \frac{N_{B,13}^{\text{lump}} N_{B,32}^{\text{lump}}}{N_{A,33}^{\text{lump}} + N_{B,33}^{\text{lump}}} \right] Th_{\partial E,3}^{n+1} \\ & + \left[\frac{-N_{A,32}^{\text{lump}} N_{B,13}^{\text{lump}}}{N_{A,33}^{\text{lump}} + N_{B,33}^{\text{lump}}} \right] Th_{\partial E,4}^{n+1} - \frac{N_{B,13}^{\text{lump}}}{N_{A,33}^{\text{lump}} + N_{B33}^{\text{lump}}} F_{A,3}^{n} \\ & - \frac{N_{B,13}^{\text{lump}}}{N_{A,33}^{\text{lump}} + N_{B,33}^{\text{lump}}} F_{B,3}^{n} + F_{B,1}^{n}. \end{aligned} \tag{110}$$

[104] With this formulation, it can be shown that the final assembled system is made of an M matrix provided the fictive triangulation is acute (angles of the triangles A and B are $<\pi/2$). This triangular subdiscretization of the quadrangles has the following advantages:

[105] 1. The procedure can be applied at convenience to some elements and not necessarily to the whole meshing. This can be interesting for nonconvex meshes which cannot

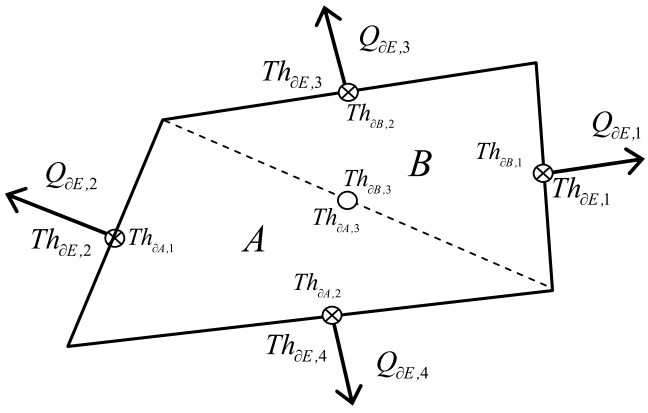

Figure 10. Subdivision of a quadrangular cell E into two triangular elements A and B.

TABLE 3. Results With the Lumped MHFE and a Small Time Step of 5 s

	Quadrangles With Standard Local Matrix		Quadrangles With the Modified Local Matrix	
Time (s)	err_g	H_{min}	err_g	H_{min}
1,600	1.1%	−1,011.2	0.07%	−1,000.0
7,600	2.0%	−1,007.	0.09%	−1,000.3
25,000	2.9%	−1,028.	0.03%	−1,000.02

be handled by the classical MHFE method. For example, the nonconvex quadrangular element can be divided in two interior triangles (A, B) by dividing the most opened angle by 2.

[106] 2. The cost is the same as for the standard approach. In both formulations (subdiscretized and standard), the final system is solved for heads at the edges of the quadrangular elements.

[107] 3. The monotonous behavior of the discretization is improved and damps unphysical oscillations.

[108] 4. The procedure is quite simple to implement since only the local matrix is changed.

[109] Table 3 illustrates how the modified local matrix can improve the solution calculated by the lumped MHFE over quadrangular meshes. With the simulations of infiltration as depicted in section 5.2, the nonphysical oscillations are strongly reduced by the proposed technique. The minimal value of head decreases from −1028 cm to −1000.3 cm, whereas the area subject to oscillations decreases from 2.9% to 0.09%. When the splitting of quadrangles generates acute triangles over the whole domain, the maximum principle is verified, and oscillations are completely removed by the new technique.

6. STREAMLINE TRACING WITH MFE

[110] Accurate tracing of streamlines and accurate computation of traveltime along these streamlines may become challenging when performed on unstructured meshes. This section discusses the benefits of MFE velocity approximations to obtain accurate streamline tracing. This discussion is based on a recent work by *Matringe et al.* [2006], who studied streamline tracing for both RT0 and BDM1 MFE methods on general triangular and quadrangular grids. Note that the same authors also applied the same technique to finite volume discretizations [*Matringe et al.*, 2008] by relying on the correspondence between MPFA and MFE methods depicted in section 4.

[111] MFEs provide an approximation of the velocity field that is especially well suited to streamline tracing [*Kaasschieter*, 1995]. A simple way to draw streamlines is by following the movement of a fluid particle in time (particle tracking). In this case, the fluid particle inside each element moves by following the MFE velocity inside the element until it reaches an exit point. This point then becomes the entry point of the downstream element. During the procedure, the residence time (time of flight) can also be stored when leaving each element.

[112] Most streamline simulators for groundwater transport are based on the Pollock method [*Pollock*, 1988]. This is a semianalytical method that recovers the exit point of a streamline and the time of flight in an element of the mesh by assuming that each component of the velocity field varies linearly inside the element. The method, initially developed for rectangles, was extended to irregular grids [*Prevost et al.*, 2002; *Jimenez et al.*, 2005] by using the Piola transform of the velocity vector from the reference element to the physical one.

[113] Since vector basis functions of the velocity are defined in the reference space, the entry point of the physical point is first mapped onto the reference space. Then the streamline is integrated in the reference space, and both the exit point and residence time are calculated. Finally, the exit point is mapped back to the physical space, and the procedure is repeated until a sink or an outflow boundary is reached.

[114] Analytical integration can be used to compute the streamline within the reference element. This integration works fine with RT0 since each component of the velocity in the reference space only depends on its own coordinates (see vector basis functions of RT0 velocity in Appendix B). This method is equivalent to the Pollock algorithm. Note, however, that the residence time can be integrated analytically only in the case of constant Jacobian $\mathbf{J}$ (i.e., when the physical element is a triangle or a parallelogram).

[115] For BDM1 velocities, the Pollock method cannot be used since each component of the velocity depends on local coordinates (see BDM1 vector basis functions in Appendix B). In this case, numerical integration is performed in time to solve the initial value problem for the streamline location $\widehat{\mathbf{x}} = \begin{pmatrix} \widehat{x} \\ \widehat{y} \end{pmatrix}$ on the reference element:

$$\begin{aligned} \varepsilon_E \frac{d\widehat{\mathbf{x}}}{dt} &= \widehat{\mathbf{q}}_E^{\text{RT0 or BDM1}}, \\ \widehat{\mathbf{x}}\left(\widehat{t} = \widehat{t}_0\right) &= \widehat{\mathbf{x}}_0, \end{aligned} \tag{111}$$

where ε_E is the porosity of the element E. In the work by *Matringe et al.* [2006], the system (111) is solved by using an explicit Runge-Kutta method of fourth order. Similarly, the residence time τ can be computed in the reference element as follows:

$$\tau = \varepsilon_E \int_{\wp} \frac{|\mathbf{J}|}{\left|\widehat{\mathbf{q}}_E^{\text{RT0 or BDM1}}\right|} \mathrm{d}s. \tag{112}$$

[116] This integral can be computed numerically within the Runge-Kutta stepping. This streamline tracing was implemented for both RT0 and BDM1 by *Matringe et al.* [2006]. The authors found that for the same computational cost, high-order tracing was more accurate and robust (less sensitive to grid orientation) than low-order tracing.

[117] As a concluding remark to this section, it must be pointed out that in the case of a cell with a sink term, the particle tracking based on MFE velocity inside the cell is not consistent [*Healy and Russell*, 2000; *Wang et al.*, 2005]. If

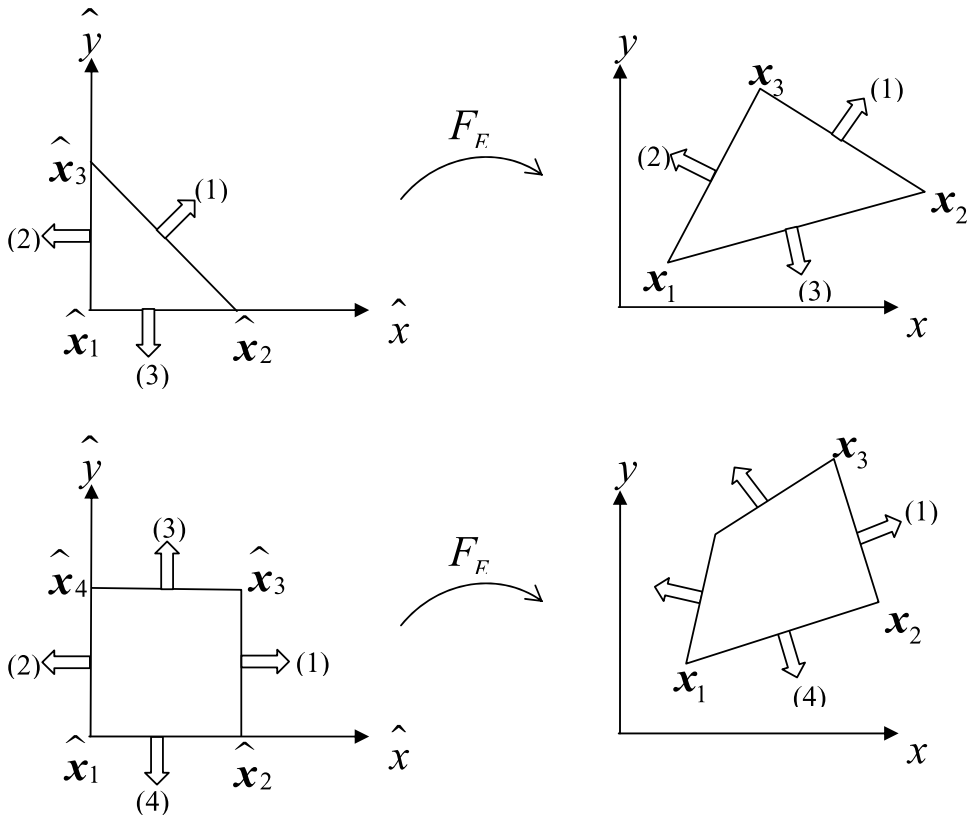

Figure A1. Mapping from the reference to the physical element for triangles and quadrangles and local numbering.

all fluxes are inflows, the velocity components are diminishing and cancel out at some point inside the element (depending on the numerical values of the fluxes). This problem is partly circumvented by using a very small cell containing the well at its center.

7. COMMENTS AND CONCLUSION

[118] MFE is an accurate method to solve diffusion-type partial differential equations. The basic idea of the method is to allow a simultaneous approximation of both the state variable and its related flux. MFE methods have received growing attention because (1) they satisfy mass conservation at the element level, (2) they provide continuous fluxes from one element to an adjacent one, (3) they preserve the same order of convergence for the state variable and the related fluxes, and (4) they are able to handle full parameter tensors and their incidence on unstructured meshes. These properties make MFEs well suited to computation problems in geosciences.

[119] Hybridization reduces the size of the standard MFE system and leads to a symmetric positive definite matrix that can be solved by efficient iterative methods. Thus, tackling problems including a large number of unknowns becomes feasible.

[120] In this paper, both RT0 and BDM1 hybrid formulations of MFEs have been presented since these methods are frequently used for practical applications. These formulations require more unknowns (one per edge or face for RT0) than standard methods (one per vertex or per cell). Many studies tried to reduce the number of unknowns and, within this context, to seek eventual links between MFEs and other numerical methods like finite volume or multipoint flux approximation methods. The MFE method is based on well-known and rigorous fundaments. Therefore, the links evoked above have provided the mathematical foundation for the numerical analysis of other methods. Along this line, MFEs helped, for instance, to bring the proof of convergence of finite differences in two dimensions

TABLE B1. BDM1 Vector Basis Functions for Triangles and Quadrangles in the Reference Element

	Triangles	Quadrangles
Edge 1	$\widehat{\omega}_{1,1}^{\mathrm{BDM1}} = 2(\hat{x},0)^T$ and $\widehat{\omega}_{1,2}^{\mathrm{BDM1}} = 2(0,\hat{y})^T$	$\widehat{\omega}_{1,1}^{\mathrm{BDM1}} = [2\hat{x}\,(1-\hat{y}), -\hat{y}\,(1-\hat{y})]^T$ and $\widehat{\omega}_{1,2}^{\mathrm{BDM1}} = [2\hat{x}\hat{y}, \hat{y}(1-\hat{y})]^T$
Edge 2	$\widehat{\omega}_{2,1}^{\mathrm{BDM1}} = 2(-\hat{y}, \hat{y})^T$ and $\widehat{\omega}_{2,2}^{\mathrm{BDM1}} = 2(\hat{x}+\hat{y}-1,0)^T$	$\widehat{\omega}_{2,1}^{\mathrm{BDM1}} = [-2(1-\hat{x})\,\hat{y}, \hat{y}(1-\hat{y})]^T$ and $\widehat{\omega}_{2,2}^{\mathrm{BDM1}} = [-2\,(1-\hat{x})\,(1-\hat{y}), -\hat{y}(1-\hat{y})]^T$
Edge 3	$\widehat{\omega}_{3,1}^{\mathrm{BDM1}} = 2(0,\,\hat{x}+\hat{y}-1)^T$ and $\widehat{\omega}_{3,2}^{\mathrm{BDM1}} = 2(\hat{x}, -\hat{x})^T$	$\widehat{\omega}_{3,1}^{\mathrm{BDM1}} = [\hat{x}(1-\hat{x}), 2\hat{x}\hat{y}]^T$ and $\widehat{\omega}_{3,2}^{\mathrm{BDM1}} = [-\hat{x}\,(1-\hat{x}), 2\hat{y}\,(1-\hat{x})]^T$
Edge 4		$\widehat{\omega}_{4,1}^{\mathrm{BDM1}} = [-\hat{x}\,(1-\hat{x}), -2(1-\hat{x})\,(1-\hat{y})]^T$ and $\widehat{\omega}_{4,2}^{\mathrm{BDM1}} = [\hat{x}\,(1-\hat{x}), -2\hat{x}(1-\hat{y})]^T$

TABLE B2. RT0 Vector Basis Functions for Triangles and Quadrangles in the Reference Element

	Triangles	Quadrangles
Edge 1	$\widehat{\omega}_1^{\mathrm{RT0}} = (\hat{x}, \hat{y})^T$	$\widehat{\omega}_1^{\mathrm{RT0}} = (\hat{x}, 0)^T$
Edge 2	$\widehat{\omega}_2^{\mathrm{RT0}} = (\hat{x} - 1, \hat{y})^T$	$\widehat{\omega}_2^{\mathrm{RT0}} = (\hat{x} - 1)^T$
Edge 3	$\widehat{\omega}_3^{\mathrm{RT0}} = (\hat{x}, \hat{y} - 1)^T$	$\widehat{\omega}_3^{\mathrm{RT0}} = (0, \hat{y})^T$
Edge 4		$\widehat{\omega}_4^{\mathrm{RT0}} = (0, \hat{y} - 1)^T$

with diagonal tensor coefficients [*Russell and Wheeler*, 1983; *Weiser and Wheeler*, 1988], of finite differences with full tensor coefficients [*Arbogast et al.*, 1997], of MPFA on 2-D quadrilaterals [*Klausen and Winther*, 2006a, 2006b], of MPFA on 2-D triangles and quadrilaterals [*Wheeler and Yotov*, 2006b], of MPFA on 3-D tetrahedrons [*Wheeler and Yotov*, 2006b], and of MPFA on 3-D hexahedrons [*Matringe et al.*, 2007, 2009].

[121] Generally, the MFE method does not satisfy the discrete maximum principle, and the resulting solution may contain unphysical oscillations. This drawback occurs for steady state problems with heterogeneous anisotropic diffusion tensor and for transient problems. In the latter case, the unphysical oscillations can be damped or avoided by the mass lumping procedure.

[122] Contrary to the standard finite volume and the multipoint flux approximation methods, the mathematical

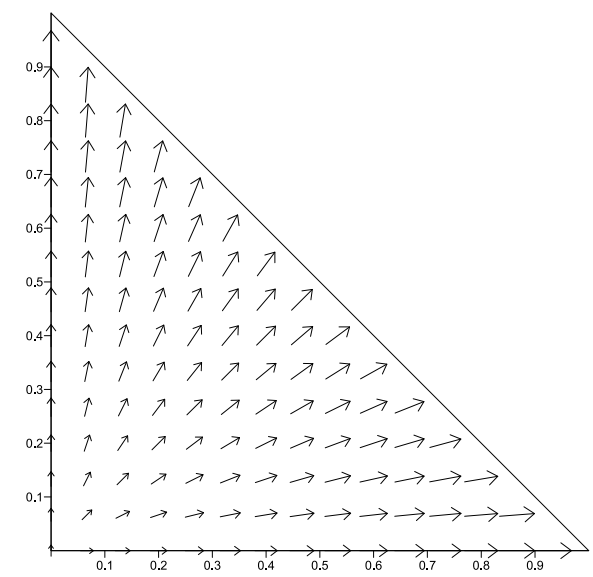

RT0 basis function $\widehat{\omega}_1^{RT0}$

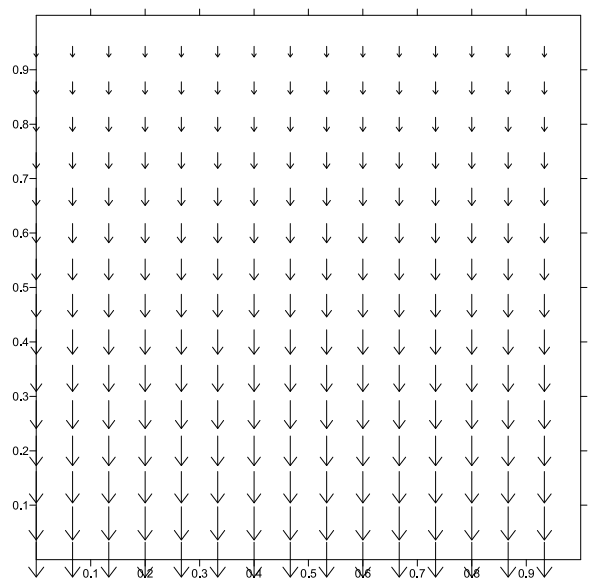

RT0 basis function $\widehat{\omega}_4^{RT0}$

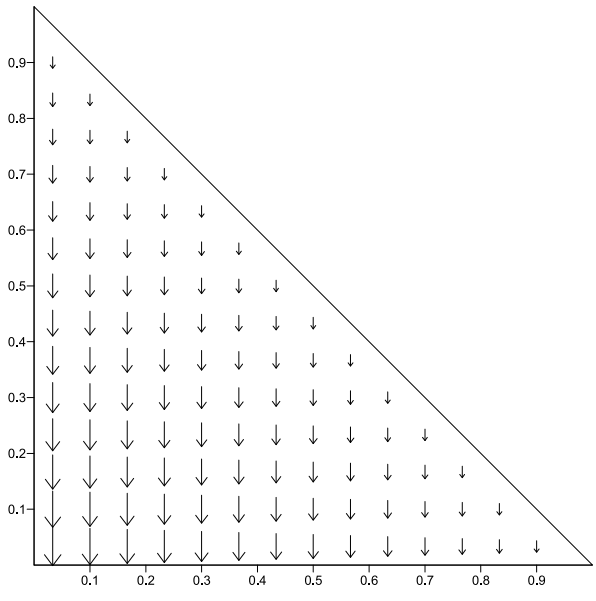

BDM1 basis function $\widehat{\omega}_{3,1}^{BDM1}$

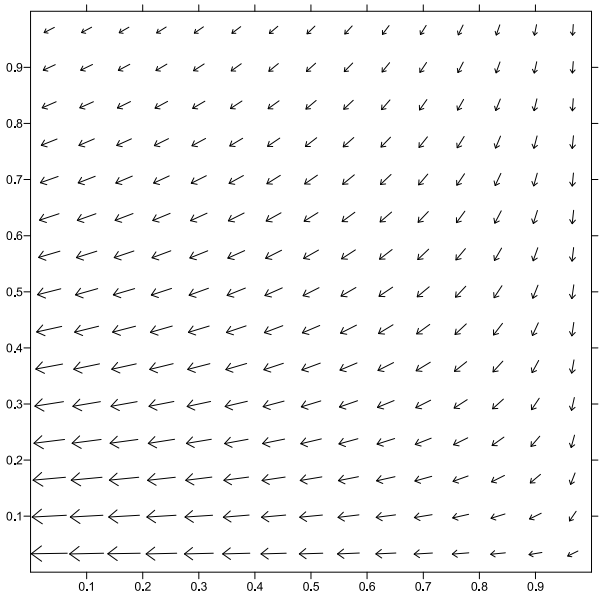

BDM1 basis function $\widehat{\omega}_{2,2}^{BDM1}$

Figure B1. RT0 and BDM1 vector basis functions for triangles and quadrangles in the reference element.

extension and implementation of MHFE to 3-D problems are not too complicated, especially with RT0 basis functions. Even in three dimensions for both regular and unstructured meshing, only local matrices have to be calculated. The resulting stencil is also smaller than with other methods since each line of the final system contains, as in two dimensions, the contribution of only two adjacent elements. However, the number of unknowns (i.e., the number of faces with RT0 basis functions) becomes much larger than the number of elements (3 times in the case of hexahedra).

APPENDIX A

[123] For any triangular element E, the mapping $F = F_E : \widehat{E} \rightarrow E$ is linear. Let $\mathbf{x}_i = (x_i, y_i)$; $i = 1, 2$, and 3 be the three vertices numbered counterclockwise of the triangle E; and $\mathbf{x}_{ij} = \mathbf{x}_i - \mathbf{x}_j$. If $\widehat{\mathbf{x}}_1 = (0, 0)^T$, $\widehat{\mathbf{x}}_2 = (1, 0)^T$, and $\widehat{\mathbf{x}}_3 = (0, 1)^T$, then (Figure A1)

$$F_E(\widehat{x}, \widehat{y}) : \mathbf{x}_1 + \mathbf{x}_{21}\widehat{x} + \mathbf{x}_{31}\widehat{y}. \tag{A1}$$

[124] For any quadrangular element E, the mapping is nonlinear. Again, let $\mathbf{x}_i = (x_i, y_i)$; $i = 1, 2, 3$, and 4 be the four vertices indexed counterclockwise of the element E; and $\mathbf{x}_{ij} = \mathbf{x}_i - \mathbf{x}_j$. If $\widehat{\mathbf{x}}_1 = (0, 0)^T$, $\widehat{\mathbf{x}}_2 = (1, 0)^T$, $\widehat{\mathbf{x}}_3 = (1, 1)^T$, and $\widehat{\mathbf{x}}_4 = (0, 1)^T$, then

$$F_E(\widehat{x}, \widehat{y}) : \mathbf{x}_1 + \mathbf{x}_{21}\widehat{x} + \mathbf{x}_{41}\widehat{y} + (\mathbf{x}_{32} - \mathbf{x}_{41})\widehat{x}\widehat{y}. \tag{A2}$$

APPENDIX B

[125] The analytical formulations of the vectorial basis function for triangular and quadrangular reference elements are given for BDM1 (see Table B1) and for RT0 (see Table B2) spaces. Two vectors of the basis function are shown in Figure B1 for triangular and rectangular elements and for both RT0 and BDM1.

[126] **ACKNOWLEDGMENTS.** This work was partly carried out within the framework of the GdR MoMas CNRS-2439 sponsored by ANDRA, BRGM, CEA, and EDF. Their support is duly acknowledged. We are grateful to the reviewers for their helpful comments and are deeply indebted to R. Juanes, who provided numerous and fruitful suggestions to improve the manuscript.

[127] The Editor responsible for this paper was Daniel Tartakovsky. He thanks three anonymous reviewers.

REFERENCES

Aarnes, J. E. (2004), On the use of a mixed multiscale finite element method for greater flexibility and increased speed or improved accuracy in reservoir simulation, *Multiscale Model. Simul.*, *2*(3), 421–439, doi:10.1137/030600655.

Aarnes, J. E., V. Kippe, and K.-A. Lie (2005), Mixed multiscale finite elements and streamline methods for reservoir simulation of large geomodels, *Adv. Water Resour.*, *28*, 257–271, doi:10.1016/j.advwatres.2004.10.007.

Aavatsmark, I. (2002), An introduction to multi-point flux approximations for quadrilateral grids, *Comput. Geosci.*, *6*, 405–432, doi:10.1023/A:1021291114475.

Aavatsmark, I., T. Barkve, Ø. Bøe, and T. Mannseth (1994), Discretization on non-orthogonal, curvilinear grids for multiphase flow, paper presented at 4th European Conference on the Mathematics of Oil Recovery, Røros, Norway.

Aavatsmark, I., T. Barkve, O. Boe, and T. Mannseth (1998a), Discretization on unstructured grids for inhomogeneous, anisotropic media. Part I: Derivation of the methods, *SIAM J. Sci. Comput.*, *19*(5), 1700–1716, doi:10.1137/S1064827595293582.

Aavatsmark, I., T. Barkve, O. Boe, and T. Mannseth (1998b), Discretization on unstructured grids for inhomogeneous, anisotropic media. Part II: Discussion and numerical results, *SIAM J. Sci. Comput.*, *19*(5), 1717–1736, doi:10.1137/S1064827595293594.

Aavatsmark, I., G. Eigestad, R. A. Klausen, M. F. Wheeler, and I. Yotov (2007), Convergence of a symmetric MPFA method on quadrilateral grids, *Comput. Geosci.*, *11*, 333–345, doi:10.1007/s10596-007-9056-8.

Ackerer, P., R. Mose, and P. Siegel (1996), Reply to comment by C. Cordes and W. Kinzelbach on "Application of the mixed hybrid finite approximation in a groundwater flow model: Luxury or necessity?," *Water Resour. Res.*, *32*(6), 1911–1913, doi:10.1029/96WR00566.

Ackerer, P., A. Younes, and R. Mosé (1999), Modeling variable density flow and solute transport in porous medium: 1. Numerical model and verification, *Transp. Porous Media*, *35*, 345–373, doi:10.1023/A:1006564309167.

Arbogast, T. (2000), Numerical subgrid upscaling of two-phase flow in porous media, in *Numerical Treatment of Multiphase Flow in Porous Media*, *Lect. Notes in Phys.*, vol. 552, edited by Z. Chen, R. E. Ewing, and Z.-C. Shi, pp. 35–49, Springer, Berlin.

Arbogast, T. (2002), Implementation of a locally conservative numerical subgrid upscaling scheme for two-phase Darcy flow, *Comput. Geosci.*, *6*(3–4), 453–481, doi:10.1023/A:1021295215383.

Arbogast, T. (2004), Analysis of a two-scale, locally conservative subgrid upscaling for elliptic problems, *SIAM J. Numer. Anal.*, *42*(2), 576–598, doi:10.1137/S0036142902406636.

Arbogast, T., and K. J. Boyd (2006), Subgrid upscaling and mixed multiscale finite elements, *SIAM J. Numer. Anal.*, *44*(3), 1150–1171, doi:10.1137/050631811.

Arbogast, T., and P. T. Kennan (1984), Mixed finite element methods as finite difference methods for solving elliptic equations on triangular elements, *Tech. Rep.*, *93-53*, Dep. of Comput. and Appl. Math., Rice Univ., Houston, Tex.

Arbogast, T., M. F. Wheeler, and I. Yotov (1997), Mixed finite elements for elliptic problems with tensor coefficients as cell centered finite differences, *SIAM J. Numer. Anal.*, *34*(2), 828–852, doi:10.1137/S0036142994262585.

Arbogast, T., C. N. Dawson, P. T. Keenan, M. F. Wheeler, and I. Yotov (1998), Enhanced cell-centered finite differences for elliptic equations on general geometry, *SIAM J. Sci. Comput.*, *19*(2), 404–425, doi:10.1137/S1064827594264545.

Arnold, D. N., R. S. Falk, and R. Winther (1997), Preconditioning in H(div) and applications, *Math. Comput.*, *66*, 957–984, doi:10.1090/S0025-5718-97-00826-0.

Baranger, J., J. F. Maitre, and F. Oudin (1994), Application de la théorie des éléments finis mixtes à l'étude d'une classe de schémas aux volumes-différences finis pour les problèmes elliptiques, *C. R. Acad. Sci., Ser. I*, *319*, 401–404.

Bause, M. (2008), Higher and lowest order mixed finite element approximation of subsurface flow problems with solutions of low regularity, *Adv. Water Resour.*, *31*, 370–382, doi:10.1016/j.advwatres.2007.09.003.

Beckie, R., E. F. Wood, and A. Aldama (1993), Mixed finite element simulation of saturated flow unsing multigrid accelerated domain decomposition technique, *Water Resour. Res.*, *29*(9), 3145–3157, doi:10.1029/93WR00931.

Belfort, B., F. Ramasomanana, A. Younes, and F. Lehmann (2009), An efficient lumped mixed hybrid finite element formu-

lation for variably saturated groundwater flow, *Vadose Zone J.*, *8*, 352–362, doi:10.2136/vzj2008.0108.

Bergamaschi, L., and M. Putti (1999), Mixed finite element methods and Newton-type linearization for the solution of Richard's equation, *Int. J. Numer. Methods Eng.*, *45*, 1025–1046.

Bergamaschi, L., S. Mantica, and F. Saleri (1994), Mixed finite element approximation of Darcy's law in porous media, *Tech. Rep.*, *CRS4*, Cagliari Univ., Cagliari, Italy.

Berndt, M., K. Lipnikov, J. Moulton, and M. Shashkov (2001), Convergence of mimetic finite difference discretizations of the diffusion equation, *East West J. Numer. Math.*, *9*, 253–316.

Bossavit, A. (1988), Mixed finite elements and the complex of Whitney forms, in *The Mathematics of Finite Elements and Applications VI*, edited by J. R. Whiteman, pp. 137–144, Academic, London.

Brezzi, F., and M. Fortin (1991), *Mixed and Hybrid Finite Element Methods*, Springer, Berlin.

Brezzi, F., J. Douglas Jr., and L. D. Marini (1985), Two families of mixed finite elements for second order elliptic problems, *Numer. Math.*, *47*, 217–235, doi:10.1007/BF01389710.

Brezzi, F., M. Fortin, and L. D. Marini (2004), Piecewise constant pressures for Darcy law, in *Finite Elements Methods: 1970 and Beyond*, edited by L. P. Franca, pp. 140–153, Int. Cent. for Numer. Methods in Eng., Barcelona.

Brezzi, F., K. Lipnikov, and V. Simoncini (2005a), A family of mimetic finite difference methods on polygonal and polyhedral meshes, *Math. Models Methods Appl. Sci.*, *15*, 1533–1553, doi:10.1142/S0218202505000832.

Brezzi, F., K. Lipnikov, and M. Shashkov (2005b), Convergence of mimetic finite difference methods for diffusion problems on polyhedral meshes, *SIAM J. Numer. Anal.*, *43*, 1872–1896, doi:10.1137/040613950.

Cai, Z., J. Jones, S. F. McCormick, and T. Russell (1997), Control volume mixed finite element methods, *Comput. Geosci.*, *1*, 289–315, doi:10.1023/A:1011577530905.

Cai, Z., J. Douglas Jr., and M. Park (2003), Development and analysis of higher order finite volume methods over rectangles for elliptic equations, *Adv. Comput. Math.*, *19*, 3–33, doi:10.1023/A:1022841012296.

Chavent, G., and J. Jaffré (1986), *Mathematical Models and Finite Elements for Reservoir Simulation*, North-Holland, Amsterdam.

Chavent, G., and J. E. Roberts (1991), A unified physical presentation of mixed, mixed hybrid finite elements and standard finite difference approximations for the determination of velocities in waterflow problems, *Adv. Water Resour.*, *14*, 329–348, doi:10.1016/0309-1708(91)90020-O.

Chavent, G., G. Cohen, and J. Jaffré (1984), Discontinuous upwinding and mixed finite elements for two-phase flows in reservoir simulation, *Comput. Methods Appl. Mech. Eng.*, *47*, 93–118, doi:10.1016/0045-7825(84)90049-5.

Chavent, G., A. Younes, and P. Ackerer (2003), On the finite volume reformulation of the mixed finite element method for elliptic and parabolic PDE on triangles, *Comput. Methods Appl. Mech. Eng.*, *192*, 655–682, doi:10.1016/S0045-7825(02)00578-9.

Chen, Q. Y., J. Wan, Y. Yang, and R. T. Mifflin (2008), Enriched multi-point flux approximation for general grids, *J. Comput. Phys.*, *227*, 1701–1721, doi:10.1016/j.jcp.2007.09.021.

Chen, Z., and R. E. Ewing (1997), From single phase to compositional flow: Applicability of mixed finite elements, *Transp. Porous Media*, *27*, 225–242, doi:10.1023/A:1006507816183.

Chen, Z., and T. Y. Hou (2002), A mixed multiscale finite element method for elliptic problems with oscillating coefficients, *Math. Comput.*, *72*(242), 541–576, doi:10.1090/S0025-5718-02-01441-2.

Chounet, L. M., D. Hilhorst, C. Jouron, Y. Kelanemer, and P. Nicolas (1999), Simulation of water flow and heat transfer in soils by means of a mixed finite element method, *Adv. Water Resour.*, *22*(5), 445–460, doi:10.1016/S0309-1708(98)00029-3.

Cirpka, O. A., R. Helmig, and E. O. Frind (1999), Numerical methods for reactive transport on rectangular and streamline-oriented grids, *Adv. Water Resour.*, *22*(7), 697–710, doi:10.1016/S0309-1708(98)00050-5.

Cordes, C., and W. Kinzelbach (1992), Continuous groundwater velocity field and path lines in linear, bilinear, and trilinear finite elements, *Water Resour. Res.*, *28*(11), 2903–2911, doi:10.1029/92WR01686.

Cordes, C., and W. Kinzelbach (1996), Comment on "Application of the mixed hybrid finite element approximation in a groundwater flow model: Luxury or necessity?" by R. Mosé, P. Siegel, P. Ackerer, and G. Chavent, *Water Resour. Res.*, *32*(6), 1905–1909, doi:10.1029/96WR00567.

Correa, M. R., and A. F. D. Loula (2007), Stabilized velocity post-processings for Darcy flow in heterogeneous porous media, *Commun. Numer. Methods Eng.*, *23*(6), 461–489, doi:10.1002/cnm.904.

Crouzeix, M., and P. A. Raviart (1973), Conforming and nonconforming finite element methods for solving the stationary Stokes equations I, *Rev. Fr. Autom. Inf. Rech. Oper. Math.*, *7*(3), 33–75.

Darlow, B. L., R. E. Ewing, and M. F. Wheeler (1984), Mixed finite elements methods for miscible displacement problems in porous media, *SPEJ Soc. Pet. Eng. J.*, *24*, 397–398, doi:10.2118/10501-PA.

Dawson, C. (1999), Conservative, shock-capturing transport methods with nonconservative velocity approximations, *Comput. Geosci.*, *3*, 205–227, doi:10.1023/A:1011539311766.

Dawson, C. N., M. F. Wheeler, and C. S. Woodward (1998), A two-grid finite difference scheme for non linear parabolic equations, *SIAM J. Numer. Anal.*, *35*(2), 435–452, doi:10.1137/S0036142995293493.

Durlofsky, L. J. (1994), Accuracy of mixed and control volume finite element approximations to Darcy velocity and related quantities, *Water Resour. Res.*, *30*, 965–973, doi:10.1029/94WR00061.

Durlofsky, L. J. (1998), Coarse scale models of two-phase flow in heterogeneous reservoirs: Volume averaged equations and their relationship to existing upscaling techniques, *Comput. Geosci.*, *2*, 73–92, doi:10.1023/A:1011593901771.

Edwards, M. (2002), Unstructured, control-volume distributed, full-tensor finite-volume schemes with flow based grids, *Comput. Geosci.*, *6*, 433–452, doi:10.1023/A:1021243231313.

Edwards, M. G., and C. F. Rogers (1994), A flux continuous scheme for the full tensor pressure equation, paper presented at 4th European Conference on the Mathematics of Oil Recovery, Røros, Norway.

Edwards, M. G., and C. F. Rogers (1998), Finite volume discretization with imposed flux continuity for the general tensor pressure equation, *Comput. Geosci.*, *2*, 259–290, doi:10.1023/A:1011510505406.

Ewing, R. E., and R. F. Heinemann (1983), Incorporation of mixed finite element methods in compositional simulation for reduction of numerical dispersion, in *Proceedings of the Seventh SPE Symposium on Reservoir Simulation, San Francisco, California*, pp. 341–347, Soc. of Pet. Eng., Richardson, Tex.

Ewing, R. E., M. Liu, and J. Wang (1999), Superconvergence of mixed finite element approximation over quadrilaterals, *SIAM J. Numer. Anal.*, *36*, 772–787, doi:10.1137/S0036142997322801.

Farthing, M. W., C. E. Kees, and C. T. Miller (2003), Mixed finite element methods and higher order temporal approximations for variably saturated flow, *Adv. Water Resour.*, *26*, 373–394, doi:10.1016/S0309-1708(02)00187-2.

Fraeijs de Veubeke, B., and M. A. Hugge (1972), Dual analysis for heat conduction problems by finite elements, *Int. J. Numer. Meth. Eng.*, *5*, 65–82.

Girault, V., and P. A. Raviart (1986), *Finite Element Methods for Navier-Stokes Equations: Theory and Algorithms*, *Springer Ser. in Comput. Math.*, vol. 5, 376 pp., Springer, Berlin.

Glass, R. J., J.-Y. Parlange, and T. S. Steenhuis (1989), Wetting front instability: 2. Experimental determination of relationships between system parameters and two-dimensional unstable flow field behaviour in initially dry porous media, *Water Resour. Res.*, *25*(6), 1195–1207, doi:10.1029/WR025i006p01195.

Glowinski, R., and P. Le Tallec (1989), *Augmented Lagrangian and Operator Splitting Methods in Nonlinear Mechanics*, Soc. for Ind. and Appl. Math., Philadelphia, Pa.

Golub, G. H., and C. F. Van Loan (1989), *Matrix Computations*, Johns Hopkins Univ. Press, Baltimore, Md.

Healy, R. W., and T. F. Russell (2000), Treatment of internal sources in the finite volume ELLAM, in *XIII International Conference on Computational Methods in Water Resources*, edited by L. R. Bentley et al., pp. 619–622, A. A. Balkema, Calgary, Alberta, Canada.

Herrman, L. R. (1967), Finite element bending analysis for plates, *J. Eng. Mech.*, *5*, 13–26.

Holstad, A. (2001), Temperature-driven fluid flow in porous media using a mixed finite element method and a finite volume method, *Adv. Water Resour.*, *24*(8), 843–862, doi:10.1016/S0309-1708(01)00012-4.

Hoteit, H., and A. Firoozabadi (2005), Multicomponent fluid flow by discontinuous Galerkin and mixed methods in unfractured and fractured media, *Water Resour. Res.*, *41*, W11412, doi:10.1029/2005WR004339.

Hoteit, H., and A. Firoozabadi (2008), Numerical modeling of two-phase flow in heterogeneous permeable media with different capillarity pressures, *Adv. Water Resour.*, *31*(1), 56–73, doi:10.1016/j.advwatres.2007.06.006.

Hoteit, H., R. Mosé, B. Philippe, P. Ackerer, and J. Erhel (2002a), About the maximum principle violations of the mixed-hybrid finite element method applied to diffusion equations, *Int. J. Numer. Methods Eng.*, *55*(12), 1373–1390, doi:10.1002/nme.531.

Hoteit, H., J. Erhel, R. Mosé, B. Philippe, and P. Ackerer (2002b), Numerical reliability for mixed methods applied to flow problems in porous media, *Comput. Geosci.*, *6*, 161–194, doi:10.1023/A:1019988901420.

Huber, R., and R. Helmig (1999), Multiphase flow in heterogeneous porous media: A classical finite element method versus an implicit pressure-explicit saturation based mixed finite element-finite volume approach, *Int. J. Numer. Methods Fluids*, *29*, 899–920, doi:10.1002/(SICI)1097-0363(19990430)29:8<899::AID-FLD715>3.0.CO;2-W.

Hughes, T. J. R., G. Engel, L. Mazzei, and M. G. Larson (2000), The continuous Galerkin method is locally conservative, *J. Comput. Phys.*, *163*, 467–488, doi:10.1006/jcph.2000.6577.

Hyman, J., M. Shashkov, and S. Steinberg (1997), The numerical solution of diffusion problems in strongly heterogeneous non-isotropic materials, *J. Comput. Phys.*, *132*, 130–148, doi:10.1006/jcph.1996.5633.

Jaffré, J., J. E. Roberts, and A. Sboui (2006), Mixed hexahedral finite elements for Darcy flow calculations, in *Proceedings of the XVI International Conference on Computational Methods in Water Resources* [electronic], Tech. Univ. of Denmark, Copenhagen. (Available at http://proceedings.cmwr-xvi.org/getFile.py/access?contribId=312&sessionId=10&resId=0&materialId=paper&confId=a051)

James, A. I., and W. D. Graham (1999), Numerical approximation of head and flux covariances in three dimensions using mixed finite elements, *Adv. Water Resour.*, *22*, 729–740, doi:10.1016/S0309-1708(98)00044-X.

Jimenez, E., K. Sabir, A. Datta-Gupta, and M. J. King (2005), Spatial error and convergence in streamline simulation, in *SPE Reservoir Simulation Symposium*, pp. 111–125, Soc. of Pet. Eng., Richardson, Tex.

Juanes, R., and F.-X. Dub (2008), A locally conservative variational multiscale method for the simulation of porous media flow with multiscale source terms, *Comput. Geosci.*, *12*(3), 273–295, doi:10.1007/s10596-007-9070-x.

Kaasschieter, E. F. (1995), Mixed finite elements for accurate particle tracking in saturated groundwater flow, *Adv. Water Resour.*, *18*(5), 277–294, doi:10.1016/0309-1708(95)00015-B.

Kaasschieter, E. F., and A. J. M. Huijben (1992), Mixed-hybrid finite elements and streamline computation for the potential flow problem, *Numer. Methods Partial Differential Equations*, *8*, 221–266, doi:10.1002/num.1690080302.

Kippe, V., J. E. Aarnes, and K.-A. Lie (2008), A comparison of multiscale methods for elliptic problems in porous media flow, *Comput. Geosci.*, *12*(3), 377–398, doi:10.1007/s10596-007-9074-6.

Klausen, R. A., and T. Russell (2005), Relations among some locally conservative discretization methods which handle discontinuous coefficients, *Comput. Geosci.*, *8*(4), 341–377, doi:10.1007/s10596-005-1815-9.

Klausen, R. A., and R. Winther (2006a), Convergence of multipoint flux approximations on quadrilateral grids, *Numer. Methods Partial Differential Equations*, *22*, 1438–1454.

Klausen, R. A., and R. Winther (2006b), Robust convergence of multi-point flux approximations on rough grids, *Numer. Math.*, *104*, 317–337.

Kuznetsov, Y., and S. Repin (2003), New mixed finite element method on polygonal and polyhedral meshes, *Russ. J. Numer. Anal. Math. Modell.*, *18*(3), 261–278, doi:10.1515/156939803322380846.

Kuznetsov, Y., and S. Repin (2005), Convergence analysis and error estimates for mixed finite element method on distorted meshes, *J. Numer. Math.*, *13*(1), 33–51, doi:10.1515/1569395054068973.

Kuznetsov, Y., K. Lipnikov, and M. Shashkov (2004), The mimetic finite difference method on polygonal meshes for diffusion-type problems, *Comput. Geosci.*, *8*, 301–324, doi:10.1007/s10596-004-3771-1.

Lipnikov, K., M. Shashkov, and D. Svyatskiy (2006), The mimetic finite difference discretization of diffusion problem on unstructured polyhedral meshes, *J. Comput. Phys.*, *211*, 473–491, doi:10.1016/j.jcp.2005.05.028.

Loula, A. F. D., F. A. Rochinha, and M. A. Murad (1995), Higher-order gradient post-processings for second-order elliptic problems, *Comput. Methods Appl. Mech. Eng.*, *128*(3–4), 361–381, doi:10.1016/0045-7825(95)00885-3.

Ma, J., G. D. Couples, and S. D. Harris (2006), A mixed finite element technique based on implicit discretization of faults for permeability upscaling in fault damage zones, *Water Resour. Res.*, *42*, W08413, doi:10.1029/2005WR004686.

Marini, L. D. (1985), An inexpensive method for the evaluation of the solution of the lowest order Raviart-Thomas mixed method, *SIAM J. Numer. Anal.*, *22*(3), 493–496, doi:10.1137/0722029.

Marini, L. D., and P. Pietra (1990), New mixed finite element schemes for current continuity equations, *Int. J. Comput. Math. Electr. Electron. Eng.*, *9*(4), 257–268.

Marsden, J. E., and T. J. R. Hughes (1983), *Mathematical Foundations of Elasticity*, Prentice Hall, Englewood Cliffs, N. J. (Reprinted with corrections, Dover, New York, 1994.)

Matringe, S. F., R. Juanes, and H. A. Tchelepi (2006), Robust streamline tracing for the simulation of porous media flow on general triangular and quadrilateral grids, *J. Comput. Phys.*, *219*(2), 992–1012, doi:10.1016/j.jcp.2006.07.004.

Matringe, S. F., R. Juanes, and H. A. Tchelepi (2007), Mixed finite element and related control volume discretizations for reservoir simulation on three-dimensional unstructured grids, in *SPE Reservoir Simulation Symposium, Houston, Texas, 26–28 February*, pp. 201–213, Soc. of Pet. Eng., Richardson, Tex.

Matringe, S. F., R. Juanes, and H. A. Tchelepi (2008), Tracing streamlines on unstructured grids from finite volume discretizations, *SPE J.*, *13*(4), 423–431.

Matringe, S. F., R. Juanes, and H. A. Tchelepi (2009), Convergence of MPFA on hexahedra, in *SPE Reservoir Simulation Sym-*

posium, Houston, Texas, 2–4 February, pp. 1293–1313, Soc. of Pet. Eng., Richardson, Tex.

Mazzia, A. (2008), An analysis of monotonicity conditions in the mixed hybrid finite element methods on unstructured triangulations, *Int. J. Numer. Methods Eng.*, *76*(3), 351–375, doi:10.1002/nme.2330.

Mlacnik, M. J., and L. J. Durlofsky (2006), Unstructured grid optimization for improved monotonicity of discrete solutions of elliptic equations with highly anisotropic coefficients, *J. Comput. Phys.*, *216*, 337–361, doi:10.1016/j.jcp.2005.12.007.

Mosé, R., P. Siegel, P. Ackerer, and G. Chavent (1994), Application of the mixed hybrid finite element approximation in a groundwater flow model: Luxury or necessity?, *Water Resour. Res.*, *30*, 3001–3012, doi:10.1029/94WR01786.

Nakshatrala, K. B., and A. J. Valocchi (2009), Non-negative mixed finite element formulations for a tensorial diffusion equation, *J. Comput. Phys.*, *228*, 6726–6752, doi:10.1016/j.jcp.2009.05.039.

Nayagum, D., G. Schäfer, and R. Mosé (2004), Modelling two phase incompressible flow in porous media using hybrid and discontinuous finite elements, *Comput. Geosci.*, *8*(1), 49–73, doi:10.1023/B:COMG.0000024446.98662.36.

Nédélec, J. C. (1980), Mixed finite element in R^3, *Numer. Math.*, *35*, 315–341, doi:10.1007/BF01396415.

Nordbotten, J. M., and G. T. Eigestad (2005), Discretization on quadrilateral grids with improved monotonicity properties, *J. Comput. Phys.*, *203*, 744–760, doi:10.1016/j.jcp.2004.10.002.

Paige, C. C., and M. A. Saunders (1975), Solution of sparse indefinite systems of linear equations, *SIAM J. Numer. Anal.*, *12*, 617–629, doi:10.1137/0712047.

Pal, M., M. G. Edwards, and A. R. Lamb (2006), Convergence study of a family of flux-continuous, finite-volume schemes for the general tensor pressure equation, *Int. J. Numer. Methods Fluids*, *51*, 1177–1203, doi:10.1002/fld.1211.

Pollock, D. W. (1988), Semianalytic computation of path lines for finite difference models, *Ground Water*, *26*, 743–750, doi:10.1111/j.1745-6584.1988.tb00425.x.

Powell, C. E. (2005), Parameter-free H(div) preconditioning for a mixed finite element formulation of diffusion problems, *IMA J. Numer. Anal.*, *25*, 783–796, doi:10.1093/imanum/dri017.

Prevost, M., M. G. Edwards, and M. J. Blunt (2002), Streamline tracing on curvilinear structured and unstructured grids, *SPE J.*, *7*(2), 139–148.

Quarteroni, A., and A. Valli (1994), *Numerical Approximation of Partial Differential Equations*, Springer, New York.

Raviart, P. A., and J. M. Thomas (1977), A mixed finite element method for second order elliptic problems, in *Mathematical Aspects of Finite Element Method, Lect. Notes in Math.*, vol. 606, pp. 292–315, Springer, New York.

Roberts, J. E., and J. M. Thomas (1989), Mixed and hybrid methods, in *Finite Element Methods (Part 1)*, edited by P. G. Ciarlet and J. L. Lions, pp. 523–639, North-Holland, Amsterdam.

Russell, T. F., and M. F. Wheeler (1983), Finite element and finite difference methods for continuous flows in porous media, in *The Mathematics of Reservoir Simulation*, edited by R. E. Ewing, pp. 35–106, Soc. for Ind. and Appl. Math., Philadelphia, Pa.

Selker, J. S., J.-Y. Parlange, and T. Steenhuis (1992), Fingered flow in two dimensions: 2. Predicting finger moisture profile, *Water Resour. Res.*, *28*(9), 2523–2528, doi:10.1029/92WR00962.

Thomas, J. M. (1977), Sur l'analyse numérique des méthodes d'eléments finis hybrides et mixtes, thèse de doctorat d'état, 311 pp., Univ. Pierre et Marie Curie, Paris.

Vohralik, M. (2004), Equivalence between mixed finite element and multi-point finite volume methods, *C. R. Acad. Sci., Ser. I*, *339*, 525–528.

Vohralik, M. (2006), Equivalence between lowest-order mixed finite element and multi-point finite volume methods on simplicial meshes, *Math. Modell. Numer. Anal.*, *40*(2), 367–391.

Wang, H., W. Zhao, and R. E. Ewing (2005), A numerical modeling of multicomponent compressible flows in porous media with multiple wells by an Eulerian-Lagrangian method, *Comput. Visual Sci.*, *8*(2), 69–81, doi:10.1007/s00791-005-0153-8.

Wang, J., and T. Mathew (1994), Mixed finite element methods over quadrilaterals, in *Proceedings of 3rd International Conference on Advances in Numerical Methods and Applications*, edited by J. T. Dimov, B. Sendov, and P. Vassilevski, pp. 203–214, World Sci., River Edge, N. J.

Weiser, A., and M. F. Wheeler (1988), On convergence of block-centered finite differences for elliptic problems, *SIAM J. Numer. Anal.*, *25*, 351–375, doi:10.1137/0725025.

Wheeler, J. A., M. F. Wheeler, and I. Yotov (2002), Enhanced velocity mixed methods for flow in multiblock domains, *Comput. Geosci.*, *6*, 315–332, doi:10.1023/A:1021270509932.

Wheeler, M. F., and I. Yotov (2006a), A cell-centered finite difference method on quadrilaterals, in *Compatible Spatial Discretizations for Partial Differential Equations*, *IMA Vol. Math. Its Appl.*, *142*, 189–208.

Wheeler, M. F., and I. Yotov (2006b), A multi-point flux mixed finite element method, *SIAM J. Numer. Anal.*, *44*, 2082–2106, doi:10.1137/050638473.

Wu, X., and R. Parashkevov (2005), Effect of grid deviation on flow solutions, in *SPE Reservoir Simulation Symposium, 31 January–2 February, Houston, Texas*, pp. 97–109, Soc. of Pet. Eng., Richardson, Tex.

Younes, A., and V. Fontaine (2008a), Efficiency of mixed finite element and multipoint flow approximation methods on quadrangular grids and highly anisotropic media, *Int. J. Numer. Methods Eng.*, *76*(3), 314–336, doi:10.1002/nme.2327.

Younes, A., and V. Fontaine (2008b), Hybrid and multi-point formulations of the lowest-order mixed methods for Darcy's flow on triangles, *Int. J. Numer. Methods Fluids*, *58*(9), 1041–1062, doi:10.1002/fld.1785.

Younes, A., P. Ackerer, and R. Mose (1999a), Modeling variable density flow and solute transport in porous medium: 2. Re-evaluation of the salt dome flow problem, *Transp. Porous Media*, *35*(3), 375–394, doi:10.1023/A:1006504326005.

Younes, A., P. Ackerer, R. Mosé, and G. Chavent (1999b), Une résolution par les éléments finis mixtes à une inconnue par maille, *C. R. Acad. Sci., Ser. I*, *328*, 623–626.

Younes, A., P. Ackerer, R. Mosé, and G. Chavent (1999c), A new formulation of the mixed finite element method for solving elliptic and parabolic PDE with triangular elements, *J. Comput. Phys.*, *149*, 148–167, doi:10.1006/jcph.1998.6150.

Younes, A., P. Ackerer, and G. Chavent (2004), From mixed finite elements to finite volumes for elliptic PDE in 2 and 3 dimensions, *Int. J. Numer. Methods Eng.*, *59*, 365–388, doi:10.1002/nme.874.

Younes, A., P. Ackerer, and F. Lehmann (2006), A new mass lumping scheme for the mixed hybrid finite element method, *Int. J. Numer. Methods Eng.*, *67*, 89–107, doi:10.1002/nme.1628.

Zheng, G., and G. D. Bennett (1995), *Applied Contaminant Transport Modeling: Theory and Practice*, 440 pp., Van Nostrand Reinhold, New York.

P. Ackerer and A. Younes, Laboratoire d'Hydrologie et de Géochimie de Strasbourg, EOST, Université de Strasbourg, CNRS, 1, rue Blessig, F-67000 Strasbourg, France. (ackerer@unistra.fr)

F. Delay, UMR 6532, University of Poitiers, CNRS, 40 Av. Recteur Pineau, F-86022 Poitiers CEDEX, France.